2

Constitutive behavior of materials

The solution of elasticity problems requires three types of relationships. First, the equilibrium equations discussed in section 1.1.2, second, the strain-displacement relationships of section 1.4.1. Finally, the stress and strain fields must be related through a set of *constitutive laws*. These constitutive laws characterize the mechanical behavior of the material and consist of a set of mathematical idealizations of their observed behavior.

Homogeneity and isotropy

Constitutive laws for homogeneous, isotropic materials will be presented first. A *homogeneous material* is a material for which the physical properties are *identical at each point* within the sample. An *isotropic material* is a material for which the physical properties are *identical in all directions*. A sample of mild steel or aluminum can usually be assumed to be both homogeneous and isotropic.

Many engineering materials, however, are neither homogeneous nor isotropic. Consider a composite material consisting of long fibers aligned along a single direction and embedded in a matrix material. Such material is not homogeneous: the properties of the fibers are, in general, very different from those of the matrix material. Furthermore, it is not isotropic: if loading is applied along the fibers, the response of the material is likely to be very different from that observed when the loading is applied in a direction transverse to the fiber orientation. Such a material is referred to as being heterogeneous and anisotropic and will be examined in the second half of this chapter.

The assumptions of homogeneity or isotropy are *scale dependent*. For instance, it seems reasonable to consider a sample of aluminum to be both homogeneous and isotropic. Of course, at the atomic level, aluminum is neither homogeneous nor isotropic. Hence, assumptions of homogeneity and isotropy only hold for samples containing a very large number of atoms.

For high temperature turbine blade applications, either poly-crystalline or single crystal materials might be used. For single crystal materials, the atoms are arranged

to form regular lattice structures that create a clearly defined orientation in the material. In such a case, a sample containing a large number of atoms could be assumed to be homogeneous but anisotropic, because the response of the material will be different when stresses are applied in different directions with respect to the lattice directions.

For poly-crystalline material samples containing a large number of crystals, the material could be considered homogeneous, but if the crystals are generally oriented in a specific direction, the material will be anisotropic. This can be the case for forged metals where the forging process aligns the crystals. For poly-crystalline material samples containing a large number of crystals arranged at random orientations with respect to each other, the material can be considered both homogeneous and isotropic, and this is often the case for common structural metals such as steel and aluminum.

For composite material reinforced with long fibers all aligned in the same direction, the material is clearly anisotropic because the fiber direction defines a preferential direction for the material. For samples containing just a few fibers, the material is not homogeneous, whereas for samples containing a very large number of fibers it is a reasonable assumption to consider the material to be homogeneous.

Material testing

At present, no first-principles based models models accurately describe the constitutive properties of structural materials. Most practical constitutive models are based on empirical data, and various types of constitutive laws have been proposed to represent the many types of experimentally observed material behaviors.

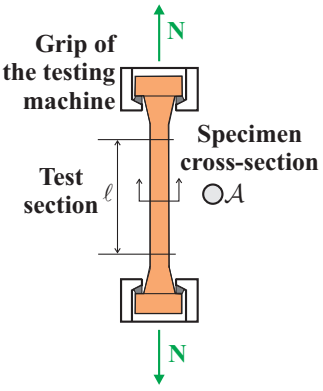

Fig. 2.1. Homogeneous bar loaded by a single stress component σ_1

If the deformation of the body remains very small, however, the stress-strain relationship can often be assumed to be linear. This widely used approximation, in which stress is proportional to strain, will be discussed in section 2.1.1. As the magnitude of the deformation increases, the stress-strain relationship can no longer be assumed to remain linear.

The stress-strain relationship for large deformations has distinctly different characteristics depending on whether the material is *ductile* or *brittle*. Constitutive relationships for ductile materials are presented in section 2.1.4 and relationships for brittle materials are presented in section 2.1.5.

Typically, material behavior is characterized by carrying out a tensile test similar to that sketched in fig. 2.1, in which a bar of circular cross-sectional area, $\mathcal{A}$, is loaded in a testing machine that applies an axial force, N, to the test specimen. The test section is a representative portion of the test specimen of length, ℓ, located at a sufficient distance away from the grips of the testing machine to avoid the end effects

they generate. The grips of the testing machine move slowly, applying an increasing load to the specimen. During the test, the extensional strain in the sample is computed by dividing the change in length of the test section by its original length, $\epsilon_1 = \Delta\ell/\ell$. The stress in the sample is computed by dividing the applied load by the sample cross-sectional area, $\sigma_1 = N/\mathcal{A}$. The results of the test are presented in the form of a stress-strain diagram: the strain is plotted along the abscissa, the stress along the ordinate.

2.1 Constitutive laws for isotropic materials

2.1.1 Homogeneous, isotropic, linearly elastic materials

For specimens undergoing small deformations, the stress-strain diagram often exhibits a linear behavior. Although this is a very crude approximation to the behavior of actual materials, it is a convenient assumption that is often used for preliminary evaluation. A linear relationship between stress and strain can be expressed as

$$\sigma_1 = E\,\epsilon_1, \tag{2.1}$$

where the coefficient of proportionality, E, is called *Young's modulus* or *modulus of elasticity*. Since strains are non-dimensional quantities, this coefficient has the same units as stress quantities, *i.e.*, Pa. This linear relationship is known as *Hooke's law*.

The elongation of a bar in the direction of the applied stress is accompanied by a lateral contraction that is also proportional to the applied stress. The resulting deformations for this uniaxial state of stress can therefore be described by the following strains

$$\epsilon_1 = \frac{1}{E}\,\sigma_1, \quad \epsilon_2 = -\frac{\nu}{E}\,\sigma_1, \quad \epsilon_3 = -\frac{\nu}{E}\,\sigma_1, \tag{2.2}$$

where ν is called *Poisson's ratio* and is a non-dimensional constant.

If a stress component, σ_2, is applied to the same material, similar deformations will result

$$\epsilon_1 = -\frac{\nu}{E}\,\sigma_2, \quad \epsilon_2 = \frac{1}{E}\,\sigma_2, \quad \epsilon_3 = -\frac{\nu}{E}\,\sigma_2. \tag{2.3}$$

Note that the assumption of material isotropy implies identical values of Young's modulus and Poisson's ratio in eq. (2.2) and (2.3). Similar relationships hold for an applied stress, σ_3.

Generalized Hooke's law

When the three stress components are applied simultaneously, the resulting deformation is the sum of the deformations obtained for each stress component applied individually because of the assumed linear behavior of the material. This results in the *generalized Hooke's law* for extensional strains

$$\epsilon_1 = \frac{1}{E}\left[\sigma_1 - \nu(\sigma_2 + \sigma_3)\right], \tag{2.4a}$$

$$\epsilon_2 = \frac{1}{E}\left[\sigma_2 - \nu(\sigma_1 + \sigma_3)\right], \tag{2.4b}$$

$$\epsilon_3 = \frac{1}{E}\left[\sigma_3 - \nu(\sigma_1 + \sigma_2)\right]. \tag{2.4c}$$

The extensional strains depend only on the direct stresses and not on the shear stresses. This is a key characteristic of isotropic materials, which does not hold for anisotropic materials.

Shear stress-shear strain relationships

The relationship between the shear strains and the shear stresses is bit more complicated to deduce, but it is revealed by the following reasoning. Consider the state of pure shear in a plane stress state described in section 1.3.5, which is characterized by two principal stresses that are equal and opposite in magnitude and with the third principal stress equal to zero. Assume that the principal stresses are $\sigma_{p2} = -\sigma_{p1}$, $\sigma_{p3} = 0$. The corresponding extensional strain components then follow from the generalized Hooke's law eq. (2.4a) and (2.4b) while the shear strain must be zero in the principal axes

$$\epsilon_1 = \frac{1+\nu}{E}\sigma_{p1}, \quad \epsilon_2 = -\frac{1+\nu}{E}\sigma_{p1}, \quad \gamma_{12} = 0. \tag{2.5}$$

In the analysis of the pure shear stress state, the state of stress on faces oriented at a 45° angle with respect to the principal stress directions is shown to take on an extreme value given by

$$\tau^*_{s12} = \sigma_{p2} = -\sigma_{p1}, \quad \sigma^*_{s1} = \sigma^*_{s2} = 0 \tag{2.6}$$

where the asterisk and subscript "s" are used to designate this special rotated axis system with maximum shear stresses. The strains in this rotated axis system are readily obtained from eq. (1.94), with $\theta_s = 45^\circ$,

$$\gamma^*_{s12} = -(\epsilon_1 - \epsilon_2) = -\frac{2(1+\nu)}{E}\,\sigma_{p1}; \quad \epsilon^*_{s1} = \epsilon^*_{s2} = 0. \tag{2.7}$$

The relationship between τ^*_{s12} and γ^*_{s12} is then obtained by comparing eq. (2.6) and eq. (2.7) above to find $\gamma^*_{s12} = -2(1+\nu)\sigma_{p1}/E = 2(1+\nu)\tau^*_{s12}/E$, or $\tau^*_{s12} = G\,\gamma^*_{s12}$, where

$$G = \frac{E}{2(1+\nu)} \tag{2.8}$$

is defined as the *shear modulus*.

The above reasoning can be repeated for a state of pure shear in the other two orthogonal planes leading to similar results for the other shear stresses and strains, and this can be summarized by the *generalized Hooke's law for shear strains*

$$\gamma_{23} = \tau_{23}/G, \quad \gamma_{13} = \tau_{13}/G, \quad \gamma_{12} = \tau_{12}/G. \tag{2.9}$$

Here again, the shear modulus is the same in all directions due to the assumed isotropy of the material.

The shear strain-shear stress relationships, eq. (2.9), are established for the case of pure shear. They remain valid, however, for more complex stress states involving axial stresses, because, in view of eq. (2.4), axial stresses create no shear strains. Similarly, the generalized Hooke's law, eq. (2.4), is established when only axial stresses are applied. They do remain valid for more complex stress states involving shear stresses because, in view of eq. (2.9), shear stresses create no axial strains.

Matrix form of the constitutive laws

The constitutive laws, eqs. (2.4) and (2.9), are often called the generalized Hooke's laws. They can be expressed in a compact matrix form as

$$\underline{\epsilon} = \underline{\underline{S}}\,\underline{\sigma}, \tag{2.10}$$

where $\underline{\epsilon}$ and $\underline{\sigma}$ are the strain and stress arrays, respectively, and store the six strain and stress components, respectively,

$$\underline{\epsilon} = \left\{\epsilon_1, \epsilon_2, \epsilon_3, \gamma_{23}, \gamma_{13}, \gamma_{12}\right\}^T, \tag{2.11a}$$

$$\underline{\sigma} = \left\{\sigma_1, \sigma_2, \sigma_3, \tau_{23}, \tau_{13}, \tau_{12}\right\}^T, \tag{2.11b}$$

and the 6×6 *material compliance matrix*, $\underline{\underline{S}}$, is defined as

$$\underline{\underline{S}} = \frac{1}{E}\left[\begin{array}{ccc|ccc} 1 & -\nu & -\nu & 0 & 0 & 0 \\ -\nu & 1 & -\nu & 0 & 0 & 0 \\ -\nu & -\nu & 1 & 0 & 0 & 0 \\ \hline 0 & 0 & 0 & 2(1+\nu) & 0 & 0 \\ 0 & 0 & 0 & 0 & 2(1+\nu) & 0 \\ 0 & 0 & 0 & 0 & 0 & 2(1+\nu) \end{array}\right]. \tag{2.12}$$

The upper left 3×3 partition of the compliance matrix represents generalized Hooke's law, eq. (2.4), whereas the lower right 3×3 partition represents the shear stress-shear strain relationships, eq. (2.9). The vanishing of the upper right and lower left partitions stems from the absence of coupling between axial stresses and shear strains, and shear stresses and axial strains, respectively.

In summary, a homogeneous, linearly elastic, isotropic material is characterized by the constitutive laws given by eqs. (2.4) and (2.9) or combined as eq. (2.10). Only two material parameters are involved in these laws, Young's modulus, E, and Poisson's ratio, ν. The shear modulus G can be evaluated from eq. (2.8).

The constitutive laws are often presented in the compliance form of eq. (2.10), *i.e.*, strains are expressed as a function of stress. A straightforward algebraic process, however, yields the stiffness form of the same constitutive laws, where stresses are expressed as a function of strains,

$$\underline{\sigma} = \underline{\underline{C}}\,\underline{\epsilon}, \tag{2.13}$$

where the 6×6 *material stiffness matrix*, $\underline{\underline{C}}$, is defined as

$$\underline{\underline{C}} = \frac{E}{(1+\nu)(1-2\nu)} \left[\begin{array}{ccc|ccc} 1-\nu & \nu & \nu & 0 & 0 & 0 \\ \nu & 1-\nu & \nu & 0 & 0 & 0 \\ \nu & \nu & 1-\nu & 0 & 0 & 0 \\ \hline 0 & 0 & 0 & \frac{1-2\nu}{2} & 0 & 0 \\ 0 & 0 & 0 & 0 & \frac{1-2\nu}{2} & 0 \\ 0 & 0 & 0 & 0 & 0 & \frac{1-2\nu}{2} \end{array}\right]. \tag{2.14}$$

Plane stress state

The state of plane stress is studied in section 1.3. It will be convenient to define stress and strain arrays that include only the relevant components of stress and strain,

$$\underline{\epsilon} = \left\{\epsilon_1, \epsilon_2, \gamma_{12}\right\}^T, \tag{2.15a}$$

$$\underline{\sigma} = \left\{\sigma_1, \sigma_2, \tau_{12}\right\}^T. \tag{2.15b}$$

For the state of plane stress, $\sigma_3 = \tau_{13} = \tau_{23} = 0$, and the stiffness matrix reduces to a 3×3 matrix,

$$\underline{\underline{C}} = \frac{E}{(1-\nu^2)} \begin{bmatrix} 1 & \nu & 0 \\ \nu & 1 & 0 \\ 0 & 0 & \frac{1-\nu}{2} \end{bmatrix}. \tag{2.16}$$

The constitutive laws for plane stress then become $\underline{\sigma} = \underline{\underline{C}}\,\underline{\epsilon}$, where stress and strain arrays are defined by eqs. (2.15), and the stiffness matrix by eq. (2.16). Note that due to Poisson's ratio effect, the strain component ϵ_3 does not vanish, $\epsilon_3 = -\nu(\sigma_1 + \sigma_2)$.

Plane strain state

For the plane strain case, $\epsilon_3 = \gamma_{13} = \gamma_{23} = 0$, the stiffness matrix again reduces to a 3×3 matrix, but now different from eq. (2.16),

$$\underline{\underline{C}} = \frac{E}{(1+\nu)(1-2\nu)} \begin{bmatrix} 1-\nu & \nu & 0 \\ \nu & 1-\nu & 0 \\ 0 & 0 & \frac{1-2\nu}{2} \end{bmatrix}. \tag{2.17}$$

The constitutive laws for plane stress then become $\underline{\sigma} = \underline{\underline{C}}\,\underline{\epsilon}$, where stress and strain arrays are defined by eqs. (2.15), and the stiffness matrix by eq. (2.17). Note that the stress component, σ_3, does not vanish due to Poisson's ratio effect, $\sigma_3 = \nu E(\epsilon_1 + \epsilon_2)/[(1+\nu)(1-2\nu)]$.

The bulk modulus

The volumetric strain is readily evaluated with the help of eq. (1.75)

$$e = \epsilon_1 + \epsilon_2 + \epsilon_3 = \frac{1-2\nu}{E}(\sigma_1 + \sigma_2 + \sigma_3) = \frac{1-2\nu}{E}\, I_1, \tag{2.18}$$

where I_1 is the first stress invariant defined by eq. (1.15a).

In the special case of an applied hydrostatic pressure, $\sigma_1 = \sigma_2 = \sigma_3 = p$, a linear relationship is found between the applied pressure and the resulting volumetric strain

$$p = \kappa\, e, \tag{2.19}$$

where

$$\kappa = \frac{E}{3(1-2\nu)}, \tag{2.20}$$

is known is the *bulk modulus* of the material. When Poisson's ratio approaches a value of $1/2$, the bulk modulus approaches infinity, implying the vanishing of the volumetric strain under an applied pressure. Such a material is called an *incompressible material*. Many types of rubber materials are nearly incompressible, and metals undergoing plastic deformations are often assumed to be nearly incompressible.

2.1.2 Thermal effects

When a sample of a material is heated, its dimensions will change. Under a change in temperature, homogeneous isotropic materials will expand equally in all directions, generating *thermal strains*, $\epsilon^t = f(\Delta T)$, where $f(\Delta T)$ is a function of the change in temperature ΔT. The volume of most materials increases when they are subjected to increased temperatures, whereas temperature decreases generally cause the material to shrink. There are, however, notable exceptions. For example, the transition from water to ice under decreasing temperature is accompanied by a volume increase.

For moderate temperature changes, it is often adequate to assume that $f(\Delta T)$ is a linear function of the temperature change, *i.e.*, $f(\Delta T) = \alpha \Delta T$, where α is the *coefficient of thermal expansion*, a positive number if the material expands under increased temperature. The thermal strain now becomes

$$\epsilon^t = \alpha \Delta T. \tag{2.21}$$

Two important aspects of thermal deformations must be emphasized. First, thermal strains are purely extensional: temperature changes do not induce shear strains. Second, thermal strains do not generate internal stresses, in contrast with mechanical strains that are related to internal stresses through the material constitutive law. An unconfined material sample subjected to a temperature change simply expands, but remains unstressed.

For homogeneous isotropic materials, the total strain is the sum of the thermal and mechanical strains. Thermal strains are the consequence of temperature changes,

whereas mechanical strains result from the application of stresses. The total strains are the superposition of the mechanical strains, given by eq. (2.4), and their thermal counterparts, given by eq. (2.21),

$$\epsilon_1 = \frac{1}{E}\left[\sigma_1 - \nu(\sigma_2 + \sigma_3)\right] + \alpha\Delta T; \tag{2.22a}$$

$$\epsilon_2 = \frac{1}{E}\left[\sigma_2 - \nu(\sigma_1 + \sigma_3)\right] + \alpha\Delta T; \tag{2.22b}$$

$$\epsilon_3 = \frac{1}{E}\left[\sigma_3 - \nu(\sigma_1 + \sigma_2)\right] + \alpha\Delta T. \tag{2.22c}$$

Because temperature changes induce no shear strains, the shear stress-shear strain relationships given by eq. (2.9) remain unchanged.

When dealing with constrained material samples, temperature changes will indirectly generate stresses in the material. For example, consider a bar constrained at its two ends by rigid walls that prevent any extension of the bar. When subjected to a temperature change, ΔT, the bar tries to expand in all directions, but the rigid walls prevent expansion of the bar along its axis, $\bar{\imath}_1$. The stress components in the transverse direction, σ_2 and σ_3, must vanish because the bar is free to expand in those directions, whereas the axial strain, ϵ_1, must vanish, due to the presence of the rigid walls. Eq. (2.22a) then implies

$$\epsilon_1 = \frac{1}{E}\left[\sigma_1\right] + \alpha\Delta T = 0,$$

and hence, $\sigma_1 = -E\alpha\Delta T$; the temperature change induces a compressive stress in the bar. Such stresses are called *thermal stresses*. If same the bar is allowed to freely expand, *i.e.*, if the end walls are removed, axial equilibrium of the bar implies $\sigma_1 = 0$ and eq. (2.22a) then yields $\epsilon_1 = \alpha\Delta T$: the temperature change induces thermal strains, but no thermal stresses.

Example 2.1. Material sample confined in a rigid circular cylinder
Consider a sample of linearly elastic, isotropic material confined in an infinitely rigid circular cylinder and subjected to an applied stress σ_3, as depicted in fig. 2.2. Because the circular cylinder cannot deform in the directions perpendicular to the applied stress direction, the corresponding strain components must vanish, $\epsilon_1 = \epsilon_2 = 0$. The first two equations of the generalized Hooke's laws, eqs. (2.4a) and (2.4b), then yield $\sigma_1 = \sigma_2 = \nu/(1-\nu)\ \sigma_3$. Introducing these results into the last of the generalized Hooke's laws, eq. (2.4c), leads to

$$\epsilon_3 = \frac{(1+\nu)(1-2\nu)}{E(1-\nu)}\ \sigma_3.$$

The apparent modulus of elasticity of the sample is defined as $E_a = \sigma_3/\epsilon_3$, and

$$E_a = \frac{(1-\nu)}{(1+\nu)(1-2\nu)}\ E.$$

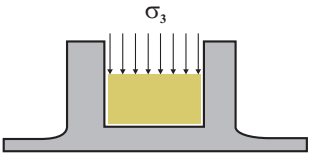

Fig. 2.2. Elastic material sample confined in a rigid circular cylinder.

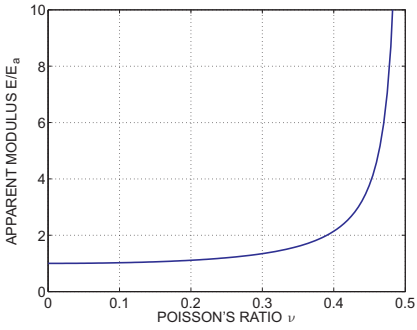

Fig. 2.3. Normalized apparent modulus of elasticity versus Poisson's ratio.

As Poisson's ratio approaches $1/2$, the normalized apparent modulus of elasticity E_a/E increases rapidly, as shown in fig. 2.3. For $\nu = 0.45$, $E_a/E = 3.79$, *i.e.*, the apparent modulus of the sample is 3.79 times that of the material.

Example 2.2. State of strain at the outer surface of a body
An experimentalist has measured the state of strain, ϵ_1, ϵ_2, and γ_{12}, at the outer surface of a three-dimensional body made of a homogeneous, isotropic, linearly elastic material. Axes $\bar{\imath}_1$ and $\bar{\imath}_2$ define the plane tangent to the outer surface of the body, and axis $\bar{\imath}_3$ is normal to this outer surface. Find the strain components ϵ_3, γ_{13} and γ_{23}.

Since the outer surface of the body is stress free, equilibrium requires $\sigma_3 = \tau_{13} = \tau_{23} = 0$. Hooke's law for shear components, see eq. (2.9), then readily implies that $\gamma_{13} = \gamma_{23} = 0$. The determination of the last strain component is more arduous. For this particular situation, generalized Hooke's laws, eqs. (2.4), become

$$\epsilon_1 = \frac{1}{E}\left[\sigma_1 - \nu\sigma_2\right], \quad \epsilon_2 = \frac{1}{E}\left[\sigma_2 - \nu\sigma_1\right], \quad \epsilon_3 = \frac{1}{E}\left[-\nu(\sigma_1 + \sigma_2)\right],$$

since $\sigma_3 = 0$. Adding together the first two equations yields $\epsilon_1 + \epsilon_2 = (1-\nu)(\sigma_1 + \sigma_2)/E$. Introducing this result in the last equation then yields

$$\epsilon_3 = -\frac{\nu}{1-\nu}(\epsilon_1 + \epsilon_2).$$

Typically, the three strain components at the outer surface of the body, ϵ_1, ϵ_2, and γ_{12}, are measured with the help of strain gauges. The determination of the remaining strain components is based on the equilibrium conditions at the surface of the body and on the constitutive laws, in this case Hooke's law.

2.1.3 Problems

Problem 2.1. Stresses expressed in terms of strains
It is sometimes necessary invert Hooke's law to express the stress in terms of the strain components. *(1)* Based on eqs. (2.4) and (2.9) prove the following relationships

$$\sigma_1 = \frac{E}{(1+\nu)(1-2\nu)}\left[(1-\nu)\epsilon_1 + \nu\epsilon_2 + \nu\epsilon_3\right], \tag{2.23a}$$

$$\sigma_2 = \frac{E}{(1+\nu)(1-2\nu)}\left[\nu\epsilon_1 + (1-\nu)\epsilon_2 + \nu\epsilon_3\right], \tag{2.23b}$$

$$\sigma_3 = \frac{E}{(1+\nu)(1-2\nu)}\left[\nu\epsilon_1 + \nu\epsilon_2 + (1-\nu)\epsilon_3\right], \tag{2.23c}$$

and

$$\tau_{12} = G\gamma_{12}, \quad \tau_{23} = G\gamma_{23}, \quad \tau_{13} = G\gamma_{13}. \tag{2.24}$$

Note: do not simply expand eq. (2.13) for your answer.

Problem 2.2. Independent coefficients for linearly elastic, isotropic materials

For a linearly elastic, isotropic material, the constitutive laws involve three parameters: Young's modulus, E, Poisson's ratio, ν, and the shear modulus, G. *(1)* Are these three coefficients independent of each other? *(2)* If not, give the equations that relate them.

Problem 2.3. Constitutive laws for stress and strain invariants

Let I_1^ϵ be the first invariant of the strain tensor, as defined by eq. (1.86), and I_1^σ be the first invariant of the stress tensor, as defined by eq. (1.15). *(1)* Find the constitutive law relating these two invariants if the material obeys the generalized Hooke's law.

Problem 2.4. Relationship between the principal stress and strain axes orientations

Prove that the principal stress and principal strain directions are always coincident at any point of a three-dimensional body made of a homogeneous, isotropic, linearly elastic material.

Problem 2.5. Stress data reduction for a strain gauge rosette

Consider the strain gauge rosette depicted in fig. 1.26A, bonded to the external surface of a body made of a homogeneous, isotropic, linearly elastic material. The following strains have been measured: $e_1 = 3657\mu$, $e_2 = -1245\mu$, $e_3 = 956\mu$. *(1)* Find the strain state at this point. *(2)* Find the principal strains and the principal strain directions at this point. *(3)* Sketch the rosette and superpose on this sketch the principal strain directions. *(4)* compute the state of stress at this point. *(5)* Find the principal stresses and the principal stress directions at this point. *(6)* Find the relationship between the principal strain and stress directions. For this material, $E = 73$ GPa and $\nu = 0.3$

Problem 2.6. Data reduction for the "stress gauge"

A "fish-bone" strain gauge has the configuration shown in fig. 2.4. The various sub-gauges, inclined at angles $+\alpha$ and $-\alpha$ with respect to the gauge direction, measure strains along those two directions, denoted ϵ_α and $\epsilon_{-\alpha}$, respectively. The sub-gauges are electrically connected in such a way that a single measurement is made, $e = \epsilon_\alpha + \epsilon_{-\alpha}$. The fish-bone gauge, also known as a "stress gauge," is intended to measure the stress, σ, along the direction of the gauge, *independently of any other stress components acting at that location*. *(1)* Find the value of angle α for which the gauge measurement, e, becomes independent of the other stress components. *(2)* Find the relationship between the measurement and the stress, σ, in the gauge direction.

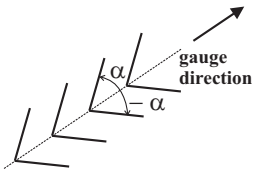

Fig. 2.4. Configuration of the "fish-bone" gauge.

2.1.4 Ductile materials

The linearly elastic behavior described in the previous section is a highly idealized behavior. In general, materials will present a nonlinear relationship between stress and strain.

Figure 2.5 shows a typical stress-strain diagram for a ductile material such as mild steel. From point **O** to point **A**, the material behaves in a linear manner, and this can be described by Hooke's law. In this region, the slope of the stress-strain diagram is constant and its value equals Young's modulus, E. If the loading is released, the specimen will come back to its original configuration without sustaining any permanent deformations, and it is referred to as being "elastic."

Beyond point **A**, the behavior is no longer proportional (linear), and hence, this point is called the *limit of proportionality*. The corresponding stress level is denoted σ_e, see fig. 2.5. The material may continue to be elastic beyond point **A**, but at some point it will begin to deform plastically, and when the load is removed, a permanent deformation will remain. The stress at which this occurs is called the *yield stress*, σ_y. More often than not, especially for mild steels, little difference exists between the limit of proportionality and the yield stress, and so σ_e and σ_y are often used interchangeably.

Beyond point **B**, the material undergoes extensive deformation at a nearly constant stress level, denoted by σ_p. From point **B** to point **C**, the material is undergoing a *plastic flow* under nearly constant stress level. Figure 2.5 shows that the strain over this region amounts to about 5% (*i.e.*, $\epsilon_1 = 0.05$), but for highly ductile steels and other materials, this may amount to more than 10%.

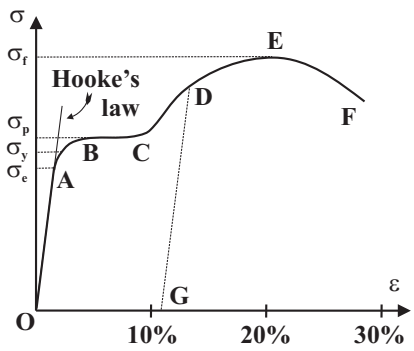

Fig. 2.5. Stress-strain diagram for a ductile material such as mild steel.

Beyond point **C**, an increasing stress level is required to continue deforming the material. The stress level increases up to point **E**, where the maximum stress level, denoted by σ_f, is reached.

Past this point, the cross-sectional area of the specimen decreases significantly at a particular location along the test section: this phenomenon is called *"necking"* of the specimen. Because the stress level is determined by dividing the applied load by the original cross-sectional area, the stress level will seem to decrease beyond point **E**, but if the stress level is computed by dividing the applied load by the reduced cross-section area of the specimen at the location where necking occurs, this *true stress* level sill continue to increase past point **E**.

With most experimental testing equipment, a controlled load (rather than a controlled deformation) is applied, and hence, point **F** is never recorded. Instead, once point **E** is reached, necking develops and the specimen breaks almost immediately afterwards. Consequently, the stress at point **E** is called the *failure stress* and desig-

nated by σ_f. Only when controlled extension is applied to the specimen is it possible to follow the behavior of the specimen from point **E** to point **F**.

Clearly, ductile materials undergo very large deformations before failure, corresponding to the portion of the stress-strain curve from point **B** to **E** in fig. 2.5. Experiments show that if the specimen is unloaded at a point between **B** and **E**, for example at point **D**, the stress-strain relationship will follow curve **DG**, parallel to **AO**, and while unloading, the material behaves elastically, although a permanent deformation of magnitude **OG** will remain after all loading is removed. If the specimen is reloaded, the stress-strain relationship will follow curve **GD**, and if additional loading is applied, it will follow curve **DEF**, as if the prior unloading had not taken place. The reloading curve **GD** is linear and reaches a higher stress level at point **D** before yield occurs and plastic deformation begins again. This increase in the yield stress is called *strain hardening*[1].

The discussion presented in the previous paragraphs is focused on diagrams of axial stress versus axial strain obtained from a tensile test as depicted in fig. 2.1. It is not unexpected that material behavior under shear exhibits nonlinear characteristics of a nature that is similar to that observed under tension. Figure 2.6 shows a typical shear stress-shear strain diagram for a ductile material such as mild steel. Here again, upon unloading, the material tends to behave in a linear manner, although a permanent deformation of magnitude **OG** will be remain after unloading.

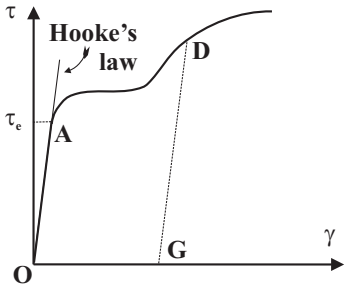

Fig. 2.6. Shear stress-shear strain diagram for a ductile material.

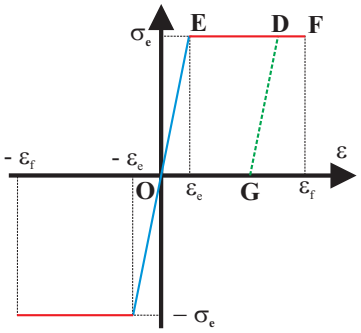

Fig. 2.7. Stress-strain diagram for an elastic-perfectly plastic material.

It is sometimes convenient to idealize the stress-strain diagram of ductile materials as presenting an initial elastic regime, followed by a perfectly plastic regime. This idealization is depicted in fig. 2.7. For a strain range $-\epsilon_e \leq \epsilon \leq \epsilon_e$, the material is linearly elastic, but for strain level outside this range, the material is *perfectly plastic*, that is, the material flows under a constant stress level, σ_e which is also the yield stress σ_y. This highly idealized material behavior is called *elastic-perfectly*

[1] Strain hardening is particularly noticeable in annealed copper such as might be encountered in new copper tubing. After the tube is initially bent, it requires a considerably greater effort to begin bending again or to try to reverse the initial bend.

plastic material behavior. Failure occurs when the strain reaches the level ϵ_f. Such a constitutive model is a good first approximation to the behavior of a ductile metallic material such as mild steel or annealed aluminum. Of course, if the material is unloaded at point **D**, the unloading curve follows segment **DG**, parallel to **OE**.

Other ductile materials such as aluminum and copper do not exhibit a plastic flow regime like the portion of the stress-strain diagram from point **B** to **C** in fig. 2.5 observed for mild steel. Figure 2.8 shows a representative stress-strain diagram for aluminum. For such materials, no pronounced limit of proportionality is present nor is the yield stress (elastic limit) evident. Instead, it is convenient to define the yield stress, denoted σ_y, as the stress level for which the specimen will exhibit a small permanent residual strain upon unloading. For aluminum, this residual strain is specified as 0.2% or $\epsilon = 0.002$. The yield stress can be determined from the stress-strain diagram by constructing a straight line parallel to the initial linearly elastic portion of the curve at a 0.2% offset and recording the stress at the intersection with the stress-strain curve, as illustrated in fig. 2.8.

2.1.5 Brittle materials

Ductile materials are characterized by stress-strain diagrams such as those presented in figs. 2.5 and 2.8: large deformations occur when stress levels greater than that corresponding to the elastic limit of the material are applied. For brittle materials, very little deformation is observed beyond the elastic limit. Typically, failure occurs abruptly at strain levels much smaller than those observed for ductile materials. Figure 2.9 shows a stress-strain diagram typical of that observed for brittle materials such as glass, concrete, stone, wood, unidirectional composites or ceramic materials.

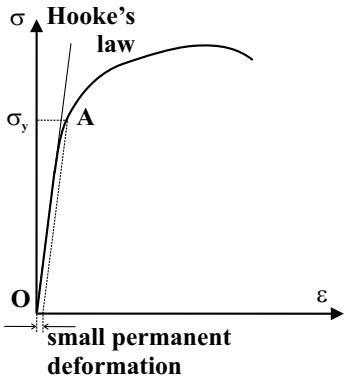

Fig. 2.8. Stress-strain diagram for a ductile material such as aluminum.

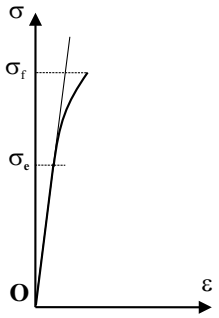

Fig. 2.9. Stress-strain diagram for a brittle material.

2.2 Allowable stress

A central problem of structural analysis is to determine the optimal configuration of a structure subjected to specific loads. The design will be influenced by many factors associated with various structural characteristics, such as those listed below.

1. *The strength of the structure*. When the local stress in the structure exceeds a specific value, the material will break or sustain permanent damage such as cracks or plastic deformations.
2. *The elastic deformation of the structure* under load. Even when subjected to small loads, a structure can present undesirable levels of elastic deformation. For example, the elastic deflection of a part may lead to interference with other parts in a structural assembly.
3. *The dynamics characteristics of the structure*. If the structure is subjected to dynamic loads, the time history of its response becomes important. More often than not, its natural frequencies must be carefully placed to avoid resonance. For aerospace structures, aeroelastic phenomena such as flutter will put stringent requirements on the torsional natural frequencies of wings and fuselages.
4. *The stability characteristics of the structure*. When parts of the structures are subjected to compressive loads, the equilibrium configuration can become unstable, resulting in buckling. During level flight, the upper skin of a wing of an aircraft is subjected to compressive loads. Wing design is significantly affected by buckling considerations.
5. *The time dependent deformations of the structure associated with creep* of the constitutive materials. Creep considerations play an important role in aircraft turbine engine design, because they are subjected to high temperatures.

The strength of a structure is the focus of the present section, although a good design must incorporate all the above characteristics. A structure is said to fail if it breaks, collapses, or develops significant permanent damage. Clearly, the applied service loads must be less, and often much less, than those corresponding to failure. The main reason for decreasing service loads is due to the numerous uncertainties about the problem. Among these are

1. The *actual magnitude of the applied service loads is not accurately known*. In an aircraft, maneuver loads or loads associated with a rough landing conditions cannot be precisely evaluated. Accidental overloads might also take place during flight or ground operations of the aircraft.
2. The *strength of materials presents statistical characteristics*. Measurements of the strengths of two nominally identical samples of aluminum will be different due to material inhomogeneities, processing difference, and experimental errors.
3. *Manufacturing variability* also plays an important role. For instance, machining fittings of complex shapes is a delicate operation. Dimensional tolerances might vary from part to part; the strength of the resulting material might not be equal to that measured in laboratory samples, and quality control sometimes fails to detect some types of defects in manufactured parts.

4. The strength of the material might decrease in time due to *corrosion, wear*, or the presence of a *chemically aggressive environment* such as salt water, fuels or solvents.
5. Finally, if failure is predicted based on the computed value of internal stresses in the structure, *these predicted stresses might be very different from their actual value*, because simplifying assumptions are used to predict these stresses.

Consequently, service loads must be limited to a conservative level, and as the uncertainty about the problem increases, so must the level of conservatism in the design. It is common practice to account for all these uncertainties by defining a *load factor*

$$\text{load factor} = \frac{\text{failure load}}{\text{service load}}, \tag{2.25}$$

where *failure load* is the load at which the part fails and *service load* is the maximum load that is expected in normal service. Of course, the load factor should be larger than unity, and it is sometimes as large as 10. Engineering judgment must be carefully exercised in choosing this load factor. If a low value is selected, the likelihood of accidental failure will increase, whereas for high values, the design might be too expensive or too heavy for its intended purpose.

The load factor might be viewed as a *factor of safety* with respect to failure: limiting the service loads to a fraction of the failure loads implies a safe operation of the structure. Using the load factor as a factor of safety is not always practical because the failure load is often unknown. Indeed, it is not practical, nor cost effective to test all structures to failure to determine the failure load. A more common approach is to compute the local stresses induced by the applied loads and limit the these local stresses to an allowable level. This can be written as

$$\text{allowable stress} = \frac{\text{yield stress}}{\text{safety factor}}, \quad \text{or} \quad \sigma_{\text{allow}} = \frac{\sigma_y}{n}, \tag{2.26}$$

where σ_{allow} is the allowable stress, σ_y the yield stress of the material, and n the factor of safety. This definition is adequate for ductile materials described in section 2.1.4. Once the yield stress is reached, permanent deformation occurs. On the other hand, for brittle materials such as those discussed in section 2.1.5, the following definition of the allowable stress is more appropriate

$$\text{allowable stress} = \frac{\text{ultimate stress}}{\text{safety factor}}, \quad \text{or} \quad \sigma_{\text{allow}} = \frac{\sigma_f}{n}, \tag{2.27}$$

where the ultimate stress is the failure stress for the material.

In summary, the stress level, σ, that a structure is subjected to during service should be smaller than the allowable stress, leading to the following strength criterion

$$|\sigma| \leq \sigma_{\text{allow}}. \tag{2.28}$$

For some materials, the allowable stress in tension and in compression are different, and the actual stress level should then be compared to the appropriate allowable stress.

2.3 Yielding under combined loading

The concept of allowable stress discussed in the previous section is focused on the highly idealized case where a structural component is subjected to a *single stress component*. The yield criterion is then simply expressed in terms of the single stress component as $\sigma \leq \sigma_y$. As depicted in fig. 1.3, a differential element of material can be subjected to a number of stress components simultaneously. The question is now: what is the proper yield criterion to be used when *multiple stress components are acting simultaneously?* Consider an aircraft propeller connected to a homogeneous, circular shaft. The engine applies a torque to the shaft resulting in shear stresses, τ, throughout the shaft. On the other hand, the propeller creates a thrust that generates uniform axial stresses, σ, over the cross-section. If the torque acts alone, the yield criterion is $\tau < \tau_y$; if the axial force acts alone, the corresponding criterion is $\sigma < \sigma_y$. In the actual structure, both stress components are acting simultaneously, and it is natural to ask: what is the proper criterion to apply?

The yield criteria to be presented in this section are applicable to isotropic, homogeneous material subjected to a general three-dimensional state of stress. Because the material is isotropic, the direction of application of the stress is irrelevant. If the material is subjected to a single stress component, it should yield under the same stress level regardless of the direction in which this stress component is applied. In contrast, if the material is anisotropic, the direction of application of stress becomes important.

For isotropic materials, there is no directional dependency of the yield criterion, even when subjected to a combined state of stress. An arbitrary state of stress can be represented by the six stress components defining the stress tensor at that point, for example, see eq. (1.3). Alternatively, the state of stress can be represented by the three principal stresses, σ_{p1}, σ_{p2}, and σ_{p3} and the three orientations defining the faces on which these principal stresses act, see section 1.2.2. If the yield criterion should not depend on directional information because of material isotropy, it is clear that *only the magnitudes of the principal stress* should appear in its expression.

In addition, empirical evidence indicates that hydrostatic stress does not cause yielding. This implies that changes in the state of stress in which the three principal stresses are increased equally will not result in yielding. Other empirical evidence also suggests that yielding is directly related to the maximum shear stress in the material which, in turn, is directly proportional to the differences between the principal stresses.

Two specific criteria will be presented here, Tresca's criterion, see section 2.3.1, and von Mises' criterion, see section 2.3.2. Both compute an equivalent maximum shear stress intensity but yield slightly different results for some cases. A more detailed discussion of yield criteria can be found in section 13.1.

2.3.1 Tresca's criterion

Tresca's yield criterion is expressed in terms of the following three principal stress inequalities

$$|\sigma_{p1} - \sigma_{p2}| \leq \sigma_y, \quad |\sigma_{p2} - \sigma_{p3}| \leq \sigma_y, \quad |\sigma_{p3} - \sigma_{p1}| \leq \sigma_y, \tag{2.29}$$

where σ_y is the yield stress observed in a uniaxial test such as that described in fig. 2.5. The material operates in the linearly elastic range when the stress state it is subjected to satisfies the three inequalities expressed by eq. (2.29). Conversely, yielding develops whenever any one of these conditions is violated. Tresca's criterion clearly meets the two conditions stated above: it depends only on the principal stresses, and a hydrostatic state of stress will not produce yielding.

Tresca's criterion can be interpreted in the following manner. Let $\overline{\imath}_1^*$, $\overline{\imath}_2^*$, and $\overline{\imath}_3^*$ be the principal stress directions. Consider now a rotation of magnitude θ about axis $\overline{\imath}_3^*$. The shear stress on this face inclined with respect to the principal stress directions is then given by eq. (1.49), where $\sigma_1 = \sigma_{p1}$, $\sigma_2 = \sigma_{p2}$ and $\tau_{12} = 0$, to yield $\tau_{12} = -(\sigma_{p1} - \sigma_{p2})/2 \sin 2\theta$. Clearly, the maximum shear stress is found on a face inclined at an angle θ = 45 degrees and gives $\tau_{12\max} = |\sigma_{p1} - \sigma_{p2}|/2$. Similar arguments for rotations about axes $\overline{\imath}_2^*$ and $\overline{\imath}_1^*$ lead to $\tau_{13\max} = |\sigma_{p1} - \sigma_{p3}|/2$, and $\tau_{23\max} = |\sigma_{p2} - \sigma_{p3}|/2$, respectively. Tresca's criterion is now recast as $\tau_{23\max} \leq \sigma_y/2$, $\tau_{13\max} \leq \sigma_y/2$ and $\tau_{12\max} \leq \sigma_y/2$.

By denoting $\tau_{\max} = \max(\tau_{23\max}, \tau_{13\max}, \tau_{12\max})$, Tresca's criterion can be expressed by a single condition, $\tau_{\max} \leq \sigma_y/2$: *the material reaches the yield condition when the maximum shear stress equals half the yield stress under a uniaxial stress state.* This physical interpretation of Tresca's criterion helps explain why it is sometimes called the *maximum shear stress criterion.* Tresca's criterion is now applied to a few combined loading cases of practical interest.

Uniaxial stress state

First, consider the case of a material subjected to an uniaxial state of stress, σ_{p1}, $\sigma_{p2} = \sigma_{p3} = 0$. The sole non-vanishing principal stress is σ_{p1}, and Tresca's yield criterion reduces to $\sigma_{p1} \leq \sigma_y$. This result is identical to the yield criterion discussed in section 2.2, as expected.

Plane state of stress

Consider a material under a plane state of stress, as defined in section 1.3. If σ_1, σ_2, and τ_{12} are the stress components in an arbitrary coordinate system, the principal stresses are readily found as

$$\sigma_{p1}, \sigma_{p2} = \frac{\sigma_1 + \sigma_2}{2} \pm \sqrt{\left(\frac{\sigma_1 - \sigma_2}{2}\right)^2 + \tau_{12}^2}, \quad \sigma_{p3} = 0. \tag{2.30}$$

Tresca's criterion now implies the following three conditions

$$2\sqrt{\left(\frac{\sigma_1 - \sigma_2}{2}\right)^2 + \tau_{12}^2} \leq \sigma_y, \quad \left|\frac{\sigma_1 + \sigma_2}{2} \pm \sqrt{\left(\frac{\sigma_1 - \sigma_2}{2}\right)^2 + \tau_{12}^2}\right| \leq \sigma_y. \tag{2.31}$$

Pure shear state

The state of pure shear is a special case of a plane stress state where $\sigma_1 = \sigma_2 = 0$ and $\tau_{12} = \tau$. The only remaining condition of Tresca's criterion, eq. (2.31), is $\tau \leq \sigma_y/2$. According to Tresca's criterion, the *shear stress level at which the material yields in a pure shear state is one half the level observed under uniaxial stress state.*

2.3.2 Von Mises' criterion

Von Mises' yield criterion is expressed by the following inequality

$$\sigma_{\text{eq}} = \frac{1}{\sqrt{2}}\sqrt{[(\sigma_{p1} - \sigma_{p2})^2 + (\sigma_{p2} - \sigma_{p3})^2 + (\sigma_{p3} - \sigma_{p1})^2]} \leq \sigma_y, \tag{2.32}$$

where the first equality defines the *equivalent stress*, σ_{eq}. Von Mises' criterion states that *the yield condition is reached under the combined loading, when the equivalent stress, σ_{eq}, reaches the yield stress for a uniaxial stress state, σ_y*. Von Mises' criterion clearly meets the requirement stated above: it only depends on the principal stresses and a hydrostatic state of stress will not produce yielding.

The physical nature of this equivalent stress is better understood by considering the octahedral face discussed in example 1.3 on page 18. The magnitude of the shear stress acting on this octahedral face is given by eq. (1.25), and simple algebra then reveals

$$3\tau_{\text{oc}}^2 = (\sigma_{p1}^2 + \sigma_{p2}^2 + \sigma_{p3}^2) - \frac{1}{3}(\sigma_{p1} + \sigma_{p2} + \sigma_{p3})^2 = \frac{2}{3}\sigma_{\text{eq}}^2. \tag{2.33}$$

This result implies that the equivalent stress is proportional the octahedral shear stress: $\sigma_{\text{eq}} = 3/\sqrt{2}\ \tau_{\text{oc}}$. Von Mises' criterion can now be restated as: *the yield condition is reached under combined loading when the octahedral shear stress reaches $3/\sqrt{2}$ of the yield stress for a uniaxial stress state, σ_y.*

When applying von Mises' criterion, the first step is to compute the equivalent stress defined by eq. (2.32). Given a loading state defined by the direct stress components σ_1, σ_2, and σ_3 and shear stress components τ_{23}, τ_{13}, and τ_{12}, it is necessary to first compute the principal stresses, σ_{p1}, σ_{p2}, and σ_{p3} using the procedure described in section 1.2.2. This laborious procedure can be bypassed by noticing that the first two invariants of the stress tensor, see eq. (1.15a) and (1.15b), can be written as $I_1 = \sigma_{p1} + \sigma_{p2} + \sigma_{p3}$ and $I_2 = \sigma_{p1}\sigma_{p2} + \sigma_{p2}\sigma_{p3} + \sigma_{p3}\sigma_{p1}$, respectively, because the shear stresses vanish on the faces normal to the principal stress directions. The following algebraic manipulations show that the equivalent stress is readily expressed in terms of these two invariant as

$$\begin{aligned}\sigma_{\text{eq}}^2 &= \left[(\sigma_{p1} - \sigma_{p2})^2 + (\sigma_{p2} - \sigma_{p3})^2 + (\sigma_{p3} - \sigma_{p1})^2\right]/2 \\ &= (\sigma_{p1}^2 + \sigma_{p2}^2 + \sigma_{p3}^2) - (\sigma_{p1}\sigma_{p2} + \sigma_{p2}\sigma_{p3} + \sigma_{p3}\sigma_{p1}) \\ &= (\sigma_{p1} + \sigma_{p2} + \sigma_{p3})^2 - 3(\sigma_{p1}\sigma_{p2} + \sigma_{p2}\sigma_{p3} + \sigma_{p3}\sigma_{p1}) = I_1^2 - 3I_2.\end{aligned} \tag{2.34}$$

If the first two stress invariants are now expressed in terms of the stress components in an arbitrarily oriented axis system using eqs. (1.15a) and (1.15b), von Mises' yield criterion can then be written as

$$\sigma_{\text{eq}} = \sqrt{\sigma_1^2 + \sigma_2^2 + \sigma_3^2 - \sigma_2\sigma_3 - \sigma_3\sigma_1 - \sigma_1\sigma_2 + 3(\tau_{23}^2 + \tau_{13}^2 + \tau_{12}^2)} \leq \sigma_y. \tag{2.35}$$

This criterion is now applied to several combined loading cases of practical interest.

Uniaxial stress state

First, consider the case of a material subjected to an uniaxial state of stress, σ_{p1}, $\sigma_{p2} = \sigma_{p3} = 0$. The sole non-vanishing principal stress is σ_{p1}, and von Mises's yield criterion reduces to $\sigma_{p1} \leq \sigma_y$. This result is identical to the yield criterion discussed in section 2.2, as expected.

Plane state of stress

Consider a material under a plane state of stress as defined in section 1.3. If σ_1, σ_2 and τ_{12} are the stress components in an arbitrary coordinate system, the equivalent stress, eq. (2.35), now reduces to

$$\sigma_{\text{eq}} = \sqrt{\sigma_1^2 + \sigma_2^2 - \sigma_1\sigma_2 + 3\tau_{12}^2} \leq \sigma_y. \tag{2.36}$$

Pure shear state

The state of pure shear is a special case of plane stress where $\sigma_1 = \sigma_2 = 0$ and $\tau_{12} = \tau$. Von Mises' criterion, eq. (2.36), reduces to $\tau \leq \sigma_y/\sqrt{3}$. According to von Mises' criterion, the shear stress level at which the material yields in a pure shear state is $1/\sqrt{3} \approx 0.577$, *i.e.*, about 60% of the level observed under uniaxial stress state. Experimentation shows that this prediction is slightly more accurate than that of Tresca's criterion. This and computational simplicity are the reasons why von Mises' criterion is more widely used than Tresca's.

2.3.3 Comparing Tresca's and von Mises' criteria

A useful geometric interpretation of Tresca's and von Mises' criteria can be obtained by considering a plane stress problem for which $\sigma_{p3} = 0$. In the stress space of the two remaining principal stresses, σ_{p1} and σ_{p2}, Tresca's criterion, see eq. (2.29), reduce to three inequalities

$$|\frac{\sigma_{p1}}{\sigma_y}| \leq 1, \quad |\frac{\sigma_{p2}}{\sigma_y}| \leq 1, \quad |\frac{\sigma_{p2}}{\sigma_y} - \frac{\sigma_{p1}}{\sigma_y}| \leq 1.$$

When taken as the limiting equalities, these three equations define the six straight line segments depicted in fig. 2.10. In the construction of this graph, the principal stresses

are normalized by the yield stress. Safe stress levels correspond to stress states falling within the irregular hexagon enclosed by the six dashed line segments. For this plane stress state, the yield envelope is therefore the hexagon shown in dashed lines in fig. 2.10.

For the same stress states, von Mises' criterion, see eq. (2.32), becomes the oblique ellipse defined by

$$\left(\frac{\sigma_{p1}}{\sigma_y}\right)^2+\left(\frac{\sigma_{p2}}{\sigma_y}\right)^2-\left(\frac{\sigma_{p1}}{\sigma_y}\right)\left(\frac{\sigma_{p2}}{\sigma_y}\right)=1.$$

Safe stress levels correspond to stress states falling within the ellipse shown in fig. 2.10 which forms the *yield envelope*.

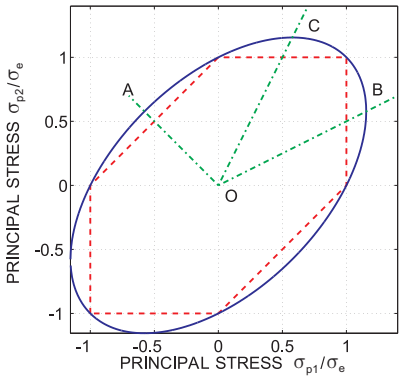

Fig. 2.10. Comparison of Tresca's and von Mises' criteria for a plane stress case.

At the six vertices of the hexagon, the yield conditions predicted by the two criteria are identical. For all other stress conditions, Tresca's criterion is slightly more conservative. In most experimental studies, yielding is observed to occur at points falling between these two criteria. As a purely practical matter, von Mises'criterion is often preferred because of its relatively simpler representation as a single analytical expression in contrast with the three separate inequalities that must be evaluated for Tresca's criterion.

When a set of loads is applied to a structure, it is natural to assume that they are all increased proportionally. Consequently, the components of the stress state, and therefore the principal stresses, increase proportionally as well. Three special stress states will be contrasted. In all three cases, the principal stresses are assumed to remain proportional as the load is applied, and hence, a single stress parameter, denoted σ, will be used to describe the loading for each case. The three stress cases are: *(1)* $\sigma_{p1} = -\sigma_{p2} = \sigma$, *(2)* $\sigma_{p1} = 2\sigma_{p2} = \sigma$, and *(3)* $\sigma_{p2} = 2\sigma_{p1} = \sigma$, and these correspond to the three radial lines **OA**, **OB**, and **OC**, respectively, shown in fig. 2.10. Table 2.1 shows a quantitative comparison of the cases. These three loading cases give the maximum discrepancy in the predictions of the two criteria. For all other loading configurations, the prediction differ by less than 15%.

Table 2.1. Comparison of the Tresca and von Mises yield criteria.

Stress state	Radial line in fig. 2.10	Tresca's yield stress	von Mises' yield stress	Percent difference
$\sigma_{p1} = -\sigma_{p2} = \sigma$	**OA**	$\sigma_y/2$	$\sigma_y/\sqrt{3}$	15.5%
$\sigma_{p1} = 2\sigma_{p2} = \sigma$	**OB**	σ_y	$2\sigma_y/\sqrt{3}$	15.5%
$\sigma_{p2} = 2\sigma_{p1} = \sigma$	**OC**	σ_y	$2\sigma_y/\sqrt{3}$	15.5%

2.3.4 Problems

Problem 2.7. Yield criterion for a confined cylindrical sample
Consider a sample of homogeneous, isotropic material of Poisson's ratio ν and yield stress σ_y confined in a rigid cylinder, as depicted in fig. 2.2. A single stress component is applied to the material and it is assumed that there is no friction between the sample and the enclosure. *(1)* Find the stress level σ_3 for which the sample will yield as a function of σ_y and ν if the material obeys Tresca's criterion. Plot your results. *(2)* Find the stress level σ_3 for which the sample will yield as a function of σ_y and ν if the material obeys von Mises' criterion. Plot your results. Use a range of Poisson's ratios $\nu \in [0,\ 0.5]$.

Problem 2.8. Yield criterion for a pressure vessel
A cylindrical pressure vessel of radius R and thickness t is subjected to an internal pressure p_i, as shown in fig. 1.20. At any point in the cylindrical portion of vessel wall, two stress components are acting: the hoop stress, $\sigma_h = Rp_i/t$ and the axial stress, $\sigma_a = Rp_i/(2t)$. The radial stress, acting in the direction perpendicular to the wall, is very small, $\sigma_r \approx 0$. The yield stress for the material is σ_y. *(1)* If the material is assumed to follow von Mises' criterion, find the maximum internal pressure the vessel can carry. *(2)* If the material is assumed to follow Tresca's criterion, find the maximum internal pressure the vessel can carry.

2.4 Material selection for structural performance

An important phase of structural design is the selection of a specific material. Table 2.2 lists the physical properties of three commonly used metals: aluminum, titanium, and steel. This table lists their respective ultimate stress, modulus of elasticity, and density. Table 2.3 lists the corresponding properties for a number of fibers.

Table 2.2 shows that the ultimate stress and modulus of elasticity of steel are far superior to those of titanium or aluminum. Why then is steel not always preferred, since it is far stronger and stiffer? A second look at table 2.2 shows that while steel is far stronger and stiffer, it is also far heavier that the other two metals. In a weight sensitive design, a compromise must be made between these conflicting characteristics. The same observations can be made when comparing the properties of fibers, as listed in table 2.3.

It is important to compare the performance of these various materials for specific structural applications. Three categories of structural design situations will be investigated, namely *strength design*, *stiffness design*, and *buckling design*. A *performance index* of the material will be derived in each case.

Table 2.2. Physical properties of a few metals.

	Ultimate stress [MPa]	Modulus of elasticity [GPa]	Density [kg/m^3]
Aluminum	620	73	2700
Titanium	1900	115	4700
Steel	4100	210	7700

Table 2.3. Physical properties of a few fibers.

	Ultimate stress [MPa]	Modulus of elasticity [GPa]	Density [kg/m^3]
E-Glass	3400	72	2550
S-Glass	4800	86	2500
Carbon	1700	190	1410
Boron	3400	400	2570
Graphite	1700	250	1410

2.4.1 Strength design

Consider a sheet of material of length L, width b, and thickness t, subjected to a tension load P, as depicted in the left portion of fig. 2.11. Assuming the stress distribution to be uniform over the sheet's cross-section, the total load the material can carry is $P_{\max} = \sigma_{\text{ult}} bt$, where σ_{ult} is the ultimate allowable stress for the material.

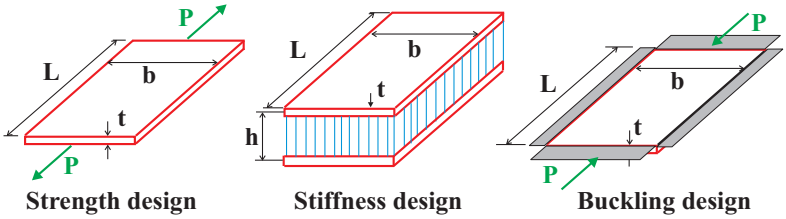

Fig. 2.11. Three types of design situation.

The total mass, M, of the structure is $M = \rho\, btL$, where ρ is the material density. Eliminating the sheet thickness between these two equations yields

$$P_{\max} = \frac{M}{L}\frac{\sigma_{\text{ult}}}{\rho}. \tag{2.37}$$

For a given mass and geometry of the structure, the maximum load it can carry is

$$P_{\max} \propto \frac{\sigma_{\text{ult}}}{\rho}. \tag{2.38}$$

The desired material performance index for strength design is σ_{ult}/ρ, and it is proportional to the maximum load that can be carried by a structure of given geometry and mass.

2.4.2 Stiffness design

In many instances, the stiffness of a structure is specified, but more often than not, it is the natural frequency of the structure that must be maximized. Consider the cantilevered, thin-walled beam of length L consisting of two thin skins of width b

and thickness t separated by a distance h as shown in the middle portion of fig. 2.11. Under certain conditions, the natural frequency of this structure is

$$\omega \propto \frac{1}{L^2}\left[\frac{H_{22}^c}{m}\right]^{1/2} \tag{2.39}$$

where H_{22}^c is the bending stiffness, and m the mass per unit span of the beam; these quantities are readily found as $H_{22}^c = Ebth^2/2[1 + 1/3(t/h)^2]$ and $m = 2\rho bt$, respectively. For a thin-walled structure $t/h \ll 1$, and the natural frequency becomes

$$\omega \propto \frac{h}{L^2}\left[\frac{E}{\rho}\right]^{1/2} \tag{2.40}$$

For a given configuration of the structure, h and L are given quantities, and the desired material performance index for stiffness design is $\sqrt{E/\rho}$, and it is proportional to the natural frequency of a structure of a given geometry and mass.

2.4.3 Buckling design

The right portion of fig. 2.11 shows a thin plate of length L, width b, and thickness t. The plate is supported around all its edges, and subjected to an in-plane compressive load P. The critical value of the load that will cause the plate to buckle is

$$P_{cr} \propto \frac{Et^3}{b}. \tag{2.41}$$

This formula will be derived in section 16.7. The total mass of the structure is $M = \rho\, btL$; eliminating the thickness of the plate from then yields

$$P_{cr} \propto \frac{M^3}{b^4L^3}\frac{E}{\rho^3}. \tag{2.42}$$

For a given mass and geometry of the structure, the desired performance index is E/ρ^3, and it is proportional to the maximum compressive load that can be carried by a structure of given geometry and mass.

Table 2.4 lists the performance indices σ_{ult}/ρ, $\sqrt{E/\rho}$, and E/ρ^3 for strength, stiffness, and buckling designs, respectively. Table 2.5 lists the corresponding quantities for a few fibers.

Consider first the data of table 2.4. Steel is clearly the best material for strength design. When it comes to stiffness design, however, the three metals perform about equally well, with only a slight disadvantage for titanium. Finally, comparing the strength and buckling designs, the ranking of the materials is now reversed: aluminum performs far better than steel and titanium in buckling design.

The same observations can be made about the fibers for which data is listed in table 2.5. In a strength design, S-glass out performs the other fibers. The situation is reversed for stiffness and buckling designs. It is clear that the third power of the

density in the denominator of the buckling design performance index makes lighter materials perform well in buckling sensitive designs.

It is not possible to directly compare the materials in tables 2.4 and 2.5. Indeed, the various metals can be used as structural materials, whereas the fibers cannot be used, as such, as structural materials. It is clear, however, that the remarkably high performance indices of these fibers justifies a closer look at their potential use in structural applications.

Table 2.4. Structural design performance indices for a few metals.

Performance index	Strength design $\sigma_{\rm ult}/\rho$ [10^3 m^2/sec^2]	Stiffness design $\sqrt{E/\rho}$ [10^3 m/sec]	Buckling design E/ρ^3 [m^8/(kg^{2}sec^2)]
Aluminum	230	5.2	3.7
Titanium	405	4.9	1.1
Steel	530	5.2	0.46

Table 2.5. Structural design performance indices for a few fibers.

Performance Index	Strength design $\sigma_{\rm ult}/\rho$ [10^3 m^2/sec^2]	Stiffness design $\sqrt{E/\rho}$ [10^3 m/sec]	Buckling design E/ρ^3 [m^8/(kg^2 sec^2)]
E-Glass	1330	5.3	4.3
S-Glass	1920	5.9	5.5
Carbon	1200	11.6	68
Boron	1320	12.5	23
Graphite	1200	13.3	89

2.5 Composite materials

2.5.1 Basic characteristics

Advanced composite materials for structural applications are made by embedding in a matrix material fibers that are all aligned in a single direction. A number of polymeric materials can be used as matrix materials. Thermoset materials such as epoxy have been extensively used as matrices for composite materials. The mechanical properties of epoxy are

$$\sigma_{\rm ult}^{\rm tens} = 50 \text{ MPa}, \quad \sigma_{\rm ult}^{\rm comp} = 140 \text{ MPa}, \tag{2.43}$$

for the ultimate allowable stress in tension and compression, respectively. The modulus of elasticity, and the density of the material are

$$E = 3.5 \text{ GPa}, \quad \rho = 1300 \text{ kg/m}^3. \tag{2.44}$$

A very crude way of approximating the strength of a composite material consisting of fibers all aligned in a single direction embedded in a matrix is to use a *rule of mixture*

$$S_c = V_f S_f + V_m S_m, \tag{2.45}$$

where S_c, S_f, and S_m are the strength of the composite, fiber, and matrix materials, respectively; and V_f and V_m the volume fractions of fiber, and matrix materials, respectively. If the material contains no voids $V_f + V_m = 1$.

Consider a composite material consisting of graphite fibers ($V_f = 0.6$), embedded in an epoxy matrix ($V_m = 0.4$). The strength of the composite can be estimated using eq. (2.45) and the data of table 2.3

$$S_c = 1700 \times 0.6 + 50 \times 0.4 = 1020 + 20 = 1040 \text{ MPa}. \tag{2.46}$$

Clearly, the matrix material contributes very little to the strength of the composite.

The stiffness of the composite can also be crudely estimated from the following reasoning. Assume the various phases of the material to be perfectly bonded together,

$$\epsilon_m = \epsilon_f = \epsilon_c, \tag{2.47}$$

where ϵ_m, ϵ_f, and ϵ_c are the strains in the matrix, fiber, and composite materials, respectively. If a sheet of this material is subjected to a tensile load P, the average stress in the composite, σ_c, can be defined as follows

$$P = A_c \sigma_c = A_f \sigma_f + A_m \sigma_m, \tag{2.48}$$

where σ_f and σ_m are the stresses in the fiber and matrix materials, respectively, and A_c, A_f, and A_m are the cross-sectional areas of composite, fiber, and matrix materials, respectively. Dividing eq. (2.48) by A_c yields

$$\sigma_c = \frac{A_f}{A_c}\sigma_f + \frac{A_m}{A_c}\sigma_m = V_f \sigma_f + V_m \sigma_m. \tag{2.49}$$

If both fiber and matrix materials are assumed to be linearly elastic, isotropic materials, the following constitutive laws adequately describe their behavior

$$\sigma_f = E_f \epsilon_f, \quad \sigma_m = E_m \epsilon_m, \tag{2.50}$$

where E_f and E_m are the moduli of elasticity for the fiber and matrix materials, respectively. Similarly, the modulus of elasticity E_c for the composite is defined as

$$\sigma_c = E_c \epsilon_c. \tag{2.51}$$

Introducing eqs. (2.50) and (2.51) into eq. (2.49), and taking into account the assumed equality of the strain in the various materials, eq. (2.47), yields

$$E_c = V_f E_f + V_m E_m. \tag{2.52}$$

For the graphite epoxy material considered above, the composite modulus of elasticity can be estimated as

$$E_c = 250 \times 0.6 + 3.5 \times 0.4 = 150 + 1.4 \approx 150 \text{ GPa}. \tag{2.53}$$

Here again, the intrinsic stiffness of the matrix material contributes little to the stiffness of the composite.

The above discussion clearly shows that a significant fraction of the high strength and stiffness of the fibers is directly inherited by the composite. The matrix material, however, contributes little to the strength and stiffness of the composite. This observation prompts the following question: what is the role of the matrix material in a composite? The matrix is needed to keep all the fibers together, and to provide an adequate surface finish. A less obvious role of the matrix is to diffuse the stresses among the otherwise isolated fibers. This aspect is explored in the next section.

2.5.2 Stress diffusion in composites

Consider a lamina consisting of fibers all aligned in a single direction embedded in a matrix material. The lamina is subjected to a far-field stress, σ_0. If all the fibers are continuous, it is easy to see how the entire load will be carried by the fibers only, with no significant contribution of the matrix. In practical situations, however, numerous broken fibers will be present in the lamina.

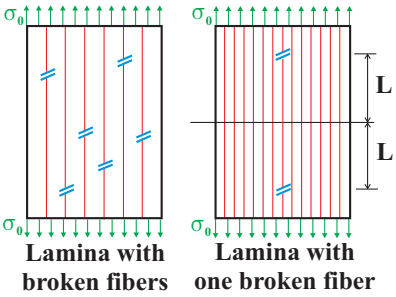

Fig. 2.12. Lamina with a broken fiber.

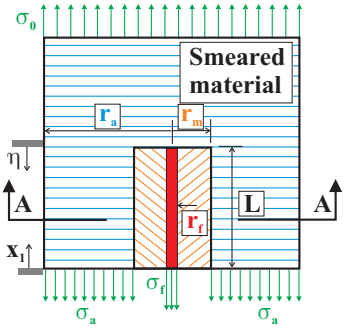

Fig. 2.13. Stress diffusion problem.

Figure 2.12 shows the geometry of the problem, including a single broken fiber of length $2L$. At the two ends of the fiber, the stress in the fiber must vanish. Nevertheless, the matrix material adjacent to the broken fiber will transfer stress from the surrounding material to the broken fiber. This stress diffusion process is a very important phenomenon because it allows *all fibers*, including broken fibers, to carry the applied load.

A simplified model of this phenomenon is depicted in the cross-section shown in fig. 2.13. It consists of a cylindrical fiber of radius r_f, surrounded by circular sleeve of matrix material of outer radius r_m, itself surrounded by a circular sleeve of composite material of outer radius r_a. The following assumptions will be made. *(1)* The matrix material carries shear stresses only. This assumption can be justified by

the fact that the stiffness of the fiber is far greater than that of the matrix, and hence, the axial stress it carries is far greater than that carried by the matrix. *(2)* The axial stress in the fiber is uniformly distributed over its cross-section. *(3)* The properties of the composite material surrounding the core fiber/matrix cylinder can *smeared*, *i.e.*, the existence of individual fibers can be ignored, except for the specific broken fiber at the heart of the model. *(4)* The various phases of the model are perfectly bonded together.

Due to the symmetry of the problem, the displacements at $x_1 = 0$ are set to zero. Figure 2.14 shows the displacements $u_f(x_1)$, and $u_a(x_1)$ of the fiber, and composite, respectively, at section A-A in fig. 2.13. The stress-displacement relationships for the various constituents of the model are

$$\epsilon_f = \frac{\mathrm{d}u_f}{\mathrm{d}x_1}, \tag{2.54a}$$

$$\epsilon_a = \frac{\mathrm{d}u_a}{\mathrm{d}x_1}, \tag{2.54b}$$

$$\gamma_m = \frac{u_a - u_f}{r_m - r_f}, \tag{2.54c}$$

where ϵ_f, ϵ_a, and γ_m are the axial strains in the fiber and composite, and the shear strain in the matrix, respectively.

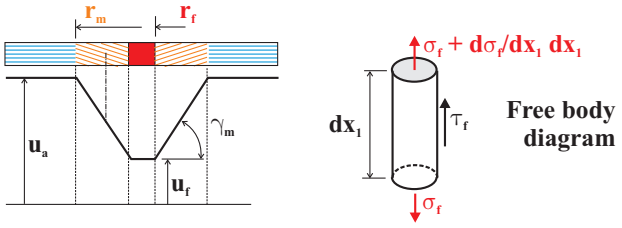

Fig. 2.14. Displacement definition and free body diagram of a differential element of fiber.

A free body diagram of a differential element of the fiber is shown in fig. 2.14. A summation of the forces along the axis of the fiber yields

$$\frac{\mathrm{d}\sigma_f}{\mathrm{d}x_1} + \frac{2}{r_f}\tau_m = 0, \tag{2.55}$$

where $\sigma_f(x_1)$ is the uniform axial stress in the fiber, and $\tau_m(x_1)$ the shear stress in the matrix. On the other hand, the free body diagram of the entire model depicted in fig. 2.13 yields an overall equilibrium equation

$$\sigma_a = \frac{\sigma_0}{1 - r_m^2/r_a^2} - \frac{r_f^2}{r_a^2}\frac{\sigma_f}{1 - r_m^2/r_a^2} \approx \sigma_0. \tag{2.56}$$

It is clear that the fiber has a much smaller radius than the overall composite, *i.e.*, $r_f/r_a \ll 1$, and the second term of this equation become negligible. Furthermore, $r_m/r_a \ll 1$, *i.e.*, $1 - (r_m/r_a)^2 \approx 1$.

If E_f, E_a, and G_m are the moduli of elasticity of the fiber, and composite, and the shearing modulus of the matrix, respectively, the constitutive laws for the various constituents of the model are

$$\sigma_f = E_f \epsilon_f, \tag{2.57a}$$
$$\sigma_a = E_a \epsilon_a, \tag{2.57b}$$
$$\tau_m = G_m \gamma_m. \tag{2.57c}$$

Introducing the matrix material constitutive law, eq. (2.57c), and the definition of the shear strain, eq. (2.54c), into the fiber equilibrium, eq. (2.55), yields

$$\frac{\mathrm{d}\sigma_f}{\mathrm{d}x_1} + \frac{2G_m}{r_f(r_m - r_f)}(u_a - u_f) = 0.$$

Taking a derivative of this equation with respect to x_1, introducing the definition of the fiber and composite strains, eqs. (2.54a) and (2.54b), respectively, and using the constitutive laws, eqs. (2.57a) and (2.57b) leads to

$$\frac{\mathrm{d}^2\sigma_f}{\mathrm{d}x_1^2} + \frac{2G_m}{r_f(r_m - r_f)}\left(\frac{\sigma_a}{E_a} - \frac{\sigma_f}{E_f}\right) = 0.$$

Finally, the stress in the composite, σ_a, is eliminated by means of the overall equilibrium eq. (2.56) to find the governing equation for the fiber stress

$$\frac{\mathrm{d}^2\sigma_f}{\mathrm{d}x_1^2} - \frac{2}{r_f(r_m - r_f)}\frac{G_m}{E_f}\sigma_f = -\frac{2}{r_f(r_m - r_f)}\frac{G_m}{E_f}\frac{E_f}{E_a}\sigma_0.$$

As shown in fig. 2.13, the non-dimensional variable $\eta = (L - x_1)/(2r_f)$ measures the distance from the fiber break divided by the fiber diameter. The governing equation for the fiber stress becomes

$$\sigma_f'' - \lambda^2\sigma_f = -\lambda^2\frac{E_f}{E_a}\sigma_0,$$

where the notation $(.)'$ is used to denote a derivative with respect to η; and $\lambda^2 = 8(G_m/E_f)(r_f/r_m)/(1 - r_f/r_m)$. The volume fraction of the material is $V_f = (\pi r_f^2)/(\pi r_m^2) = (r_f/r_m)^2$. Furthermore, the rule of mixture for the modulus of elasticity, eq. (2.52), yields $E_f/E_a = E_f/(V_f E_f + V_m E_m) \approx E_f/(V_f E_f) = 1/V_f$, where the fact that $E_m \ll E_f$ is taken into account. The governing equation finally can be recast as

$$\sigma_f'' - \lambda^2\sigma_f = -\lambda^2\frac{\sigma_0}{V_f}, \tag{2.58}$$

where

$$\lambda^2 = 8\frac{G_m}{E_f}\frac{\sqrt{V_f}}{1 - \sqrt{V_f}}. \tag{2.59}$$

The boundary conditions are $\sigma_f = 0$ at the broken end of the fiber, *i.e.*, at $\eta = 0$. At $\eta = L/2r_f$, the symmetry of the problem requires $\sigma_f' = 0$. The solution of eq. (2.58) subjected to these boundary conditions is

$$\frac{\sigma_f}{\sigma_0} = \frac{1}{V_f}\left(1 - \frac{\cosh\lambda(L/2r_f - \eta)}{\cosh(\lambda L/2r_f)}\right) \approx \frac{1}{V_f}\left(1 - e^{-\lambda\eta}\right). \tag{2.60}$$

To illustrate the distribution of stress near a fiber break, three material systems will be considered. Table 2.6 lists the relevant parameters for the three material systems: boron, graphite, and kevlar fibers in an epoxy matrix with a shearing modulus of 1.35 GPa.

Table 2.6. Physical properties of three material systems.

Material system	Volume fraction	E_f [GPa]	λ, Eq. (2.59)	δ/d_f, Eq. (2.62)
Boron/Epoxy	0.5	400	0.255	11
Graphite/Epoxy	0.6	250	0.385	7.3
Kevlar/Epoxy	0.6	130	0.534	5.3

The fiber stress at a large distance from the fiber break can be obtained from eq. (2.49): $\sigma_0 = V_f\sigma_{f\infty} + (1 - V_f)\sigma_{m\infty} \approx V_f\sigma_{f\infty}$. The stress distribution, eq. (2.60), then becomes

$$\frac{\sigma_f}{\sigma_{f\infty}} = 1 - e^{-\lambda\eta}, \tag{2.61}$$

where the notation $(.)_\infty$ is used to denote the value of the corresponding quantity at a large distance from the fiber break. The non-dimensional parameter, λ, characterizes the fiber axial stress distribution near the fiber break, which is plotted in fig. 2.15 for the three material systems. At $\eta = 0$, which corresponds to the fiber break, the fiber axial stress vanishes. The fiber axial stress grows rapidly to its far field value $\sigma_{f\infty}$.

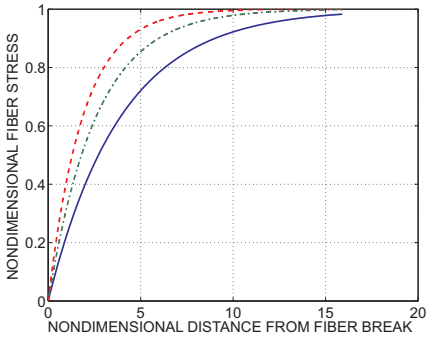

Fig. 2.15. Distribution of fiber axial stress near a fiber break for three material systems.

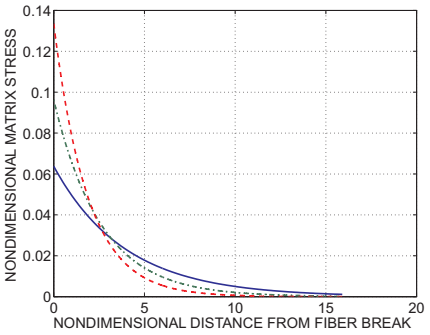

Fig. 2.16. Distribution of matrix shear stress near a fiber break for three material systems.

It is convenient to define the fiber *ineffective length* δ as the distance it takes for the fiber stress to reach 95% of its far field value, *i.e.*, $0.95 = 1 - \exp(-\lambda\delta/d_f)$, where d_f is the fiber diameter. Solving this equation yields the ineffective length as

$$\frac{\delta}{d_f} \approx \left[\frac{E_f}{G_m} \frac{1 - \sqrt{V_f}}{\sqrt{V_f}} \right]^{1/2} . \tag{2.62}$$

The ineffective length can be thought of as the length of fiber, near a fiber break, that does not carry axial stress at full capacity. Table 2.6 lists the ineffective length for the three material systems. It appears that 5.3 fiber diameters away from a break, the Kevlar fiber is already carrying 95% of its far field stress. This means that the matrix material transfers the load from the surrounding material to the broken fiber *very rapidly*. This mechanism is called the *shear lag* mechanism because the shear stress in the matrix is effectively transferring the load to the fiber. The shear stress in the matrix can be readily evaluated from the fiber equilibrium equation (2.55) as

$$\frac{\tau_m}{\sigma_{f\infty}} = \frac{\lambda}{4} e^{-\lambda \eta}. \tag{2.63}$$

Figure 2.16 shows the distribution of shear stress in the matrix near a fiber break, for the three material systems. The shear stress is maximum near the fiber break, then decays very rapidly.

An important role of the matrix material now becomes apparent in light of the above analysis. Near a fiber break, the matrix material transfers stresses from the surrounding material to the broken fiber. The shearing of the matrix near the fiber break is the mechanism that allows this stress transfer to occur. This mechanism is very efficient: for the material systems described above, the broken fiber is fully loaded within about ten fiber diameters from the fiber break. The zone affected by the fiber break is about 2δ in length (δ on each side of the break). For a graphite fiber with a diameter of 10 microns, the zone affected by a fiber break is therefore only about 200 microns in length.

Another way of looking at this fact is to say that a fiber is continuous or *infinitely long*, if its total length is much larger, say 100 times larger, than its ineffective length. Hence, a 10 micron diameter graphite fiber can be considered continuous or infinitely long when its length is greater than $100 \times 100\ 10^{-6} = 10$ mm. From a load carrying stand point, a 10 millimeter long graphite fiber can be considered continuous or infinitely long.

2.6 Constitutive laws for anisotropic materials

Section 2.1 focuses on the constitutive behavior of isotropic materials. Due to the growing importance of composite materials, the linearly elastic behavior of anisotropic materials will be addressed here. The physical properties of anisotropic materials are directional, *i.e.*, the physical response of the material depends on the direction in which it is acted upon.

Consider, as an example, the stiffness of the unidirectional composite material described in section 2.5: in the fiber direction the stiffness of the composite is dominated by the high stiffness of the fiber, see eq. (2.52). In the direction transverse

to the fiber, however, the stiffness of the composite is dominated by that of the matrix material, which is far small than that of the fiber. This contrasts with isotropic materials for which the mechanical response is identical in all directions.

The straining of the material will be measured by the engineering strain components which are stored in array $\underline{\epsilon}$, defined by eq. (2.11a). Similarly, the state of stress in the material is measured by the engineering stress components stored in array $\underline{\sigma}$, defined by eq. (2.11b). A linearly elastic, anisotropic material is characterized a linear relationship between the stress and strain measures,

$$\underline{\sigma} = \underline{\underline{C}}\,\underline{\varepsilon}; \quad \underline{\varepsilon} = \underline{\underline{S}}\,\underline{\sigma}, \tag{2.64}$$

where $\underline{\underline{C}}$ is the 6×6 *stiffness matrix* and $\underline{\underline{S}}$ the 6×6 *compliance matrix*. These two matrices are the inverse of each other, *i.e.*,

$$\underline{\underline{S}} = \underline{\underline{C}}^{-1}. \tag{2.65}$$

The strain energy, A, stored in a differential element of the material is

$$A = \frac{1}{2}\,\underline{\varepsilon}^T\underline{\sigma} = \frac{1}{2}\,\underline{\varepsilon}^T\underline{\underline{C}}\,\underline{\varepsilon} = \frac{1}{2}\,\underline{\sigma}^T\underline{\underline{S}}\,\underline{\sigma}. \tag{2.66}$$

The stored strain energy is a positive quantity for whatever deformation or stress state the material is subjected to. This implies that both stiffness and compliance matrices are symmetric and definite positive.

In general, the 6×6 stiffness matrix has $6\times 6 = 36$ independent coefficients. The symmetry requirement, however, reduces the number of independent coefficients to 21. The stress-strain relationship, eq. (2.64), written in expanded form is

$$\begin{Bmatrix} \sigma_1 \\ \sigma_2 \\ \sigma_3 \\ \tau_{23} \\ \tau_{13} \\ \tau_{12} \end{Bmatrix} = \begin{bmatrix} C_{11} & C_{12} & C_{13} & C_{14} & C_{15} & C_{16} \\ & C_{22} & C_{23} & C_{24} & C_{25} & C_{26} \\ & & C_{33} & C_{34} & C_{35} & C_{36} \\ & & & C_{44} & C_{45} & C_{46} \\ & & & & C_{55} & C_{56} \\ sym & & & & & C_{66} \end{bmatrix} \begin{Bmatrix} \epsilon_1 \\ \epsilon_2 \\ \epsilon_3 \\ \gamma_{23} \\ \gamma_{13} \\ \gamma_{12} \end{Bmatrix}, \tag{2.67}$$

where the entries in the lower triangular part of the stiffness matrix are equal to the corresponding upper triangular entries. The 21 constants, C_{ij}, characterize the behavior of the material. Each constant must be determined experimentally. A material characterized by relationship (2.67) is called an *anisotropic* or *triclinic* material.

Materials sometimes possess a plane of symmetry. Let plane $(\bar{\imath}_1, \bar{\imath}_2)$ be a plane of symmetry of the material. The stress-strain relationship reduces to

$$\begin{Bmatrix} \sigma_1 \\ \sigma_2 \\ \sigma_3 \\ \tau_{23} \\ \tau_{13} \\ \tau_{12} \end{Bmatrix} = \begin{bmatrix} C_{11} & C_{12} & C_{13} & 0 & 0 & C_{16} \\ & C_{22} & C_{23} & 0 & 0 & C_{26} \\ & & C_{33} & 0 & 0 & C_{36} \\ & & & C_{44} & C_{45} & 0 \\ & & & & C_{55} & 0 \\ sym & & & & & C_{66} \end{bmatrix} \begin{Bmatrix} \epsilon_1 \\ \epsilon_2 \\ \epsilon_3 \\ \gamma_{23} \\ \gamma_{13} \\ \gamma_{12} \end{Bmatrix}. \tag{2.68}$$

The stiffness coefficient, C_{14}, must vanish, because, if it does not vanish, an axial strain, ϵ_1, would give rise to a shear stress, τ_{23}. The presence of a shear stress, τ_{23}, however, would violate the symmetry of the response, which is a natural consequence of the material symmetry. A systematic application of this symmetry argument shows that the 8 coefficients indicated as "0" in eq. (2.68) must vanish, leaving $21 - 8 = 13$ independent coefficients. This type of material is called a *monoclinic* material.

Some materials show a higher level of symmetry characterized by two mutually orthogonal planes of symmetry; for instance, let planes $(\bar{\imath}_1,\ \bar{\imath}_2)$ and $(\bar{\imath}_2,\ \bar{\imath}_3)$ be planes of symmetry. The stress-strain relationships then reduces to

$$\begin{Bmatrix} \sigma_1 \\ \sigma_2 \\ \sigma_3 \\ \tau_{23} \\ \tau_{13} \\ \tau_{12} \end{Bmatrix} = \begin{bmatrix} C_{11} & C_{12} & C_{13} & 0 & 0 & 0 \\ & C_{22} & C_{23} & 0 & 0 & 0 \\ & & C_{33} & 0 & 0 & 0 \\ & & & C_{44} & 0 & 0 \\ & & & & C_{55} & 0 \\ sym & & & & & C_{66} \end{bmatrix} \begin{Bmatrix} \epsilon_1 \\ \epsilon_2 \\ \epsilon_3 \\ \gamma_{23} \\ \gamma_{13} \\ \gamma_{12} \end{Bmatrix}. \tag{2.69}$$

Here again symmetry arguments can be used to prove that the 12 coefficients indicated as "0" in the above matrix must vanish, leaving $21 - 12 = 9$ independent coefficients. This type of material is called an *orthotropic* material.

A case of particular importance to the study of laminated composite materials is that of materials presenting two orthogonal planes of symmetry, and one plane of isotropy. Let planes $(\bar{\imath}_1, \bar{\imath}_2)$ and $(\bar{\imath}_2, \bar{\imath}_3)$ be the mutually orthogonal planes of symmetry, and let the material be isotropic in plane $(\bar{\imath}_2, \bar{\imath}_3)$. This means, for instance, that the coefficients C_{12} and C_{13} should be identical due to the isotropic response of the material in plane $(\bar{\imath}_2, \bar{\imath}_3)$. The stress-strain relationships now reduce to

$$\begin{Bmatrix} \sigma_1 \\ \sigma_2 \\ \sigma_3 \\ \tau_{23} \\ \tau_{13} \\ \tau_{12} \end{Bmatrix} = \begin{bmatrix} C_{11} & C_{12} & C_{12} & 0 & 0 & 0 \\ & C_{22} & C_{23} & 0 & 0 & 0 \\ & & C_{22} & 0 & 0 & 0 \\ & & & \frac{C_{22}-C_{23}}{2} & 0 & 0 \\ & & & & C_{55} & 0 \\ sym & & & & & C_{55} \end{bmatrix} \begin{Bmatrix} \epsilon_1 \\ \epsilon_2 \\ \epsilon_3 \\ \gamma_{23} \\ \gamma_{13} \\ \gamma_{12} \end{Bmatrix}. \tag{2.70}$$

Only five constants remain for this material called *transversely isotropic*.

Finally, an *isotropic* material is characterized by an identical response in all directions, leading to the following stress-strain relationship

$$\begin{Bmatrix} \sigma_1 \\ \sigma_2 \\ \sigma_3 \\ \tau_{23} \\ \tau_{13} \\ \tau_{12} \end{Bmatrix} = \begin{bmatrix} C_{11} & C_{12} & C_{12} & 0 & 0 & 0 \\ & C_{11} & C_{12} & 0 & 0 & 0 \\ & & C_{11} & 0 & 0 & 0 \\ & & & \frac{C_{11}-C_{12}}{2} & 0 & 0 \\ & & & & \frac{C_{11}-C_{12}}{2} & 0 \\ sym & & & & & \frac{C_{11}-C_{12}}{2} \end{bmatrix} \begin{Bmatrix} \epsilon_1 \\ \epsilon_2 \\ \epsilon_3 \\ \gamma_{23} \\ \gamma_{13} \\ \gamma_{12} \end{Bmatrix}. \tag{2.71}$$

Two independent constants only are left for this type of material. Relations (2.67) to (2.71) give the structure of the stiffness matrix, $\underline{\underline{C}}$, for various types of materials. The compliance matrix, $\underline{\underline{S}}$ can be obtained by inversion, see eq. (2.65).

While the actual structure of the stiffness matrix is obtained based on energy and symmetry arguments, the physical interpretation of the various terms appearing in this matrix is not clear. For example, isotropic materials are shown to be characterized by two independent coefficients, C_{11} and C_{12}; in practice, isotropic materials are generally characterized by their Young's modulus and Poisson's ratio, which have a clear physical interpretation. These constants are called the *engineering constants* because they can be readily measured experimentally. For the various types of materials, the stiffness and compliance terms can be expressed in terms of the engineering constants. The following section discusses the experimental determination and the physical interpretation of the engineering constants for a lamina made of unidirectional fibers embedded in a matrix material.

2.6.1 Constitutive laws for a lamina in the fiber aligned triad

Consider a thin sheet of composite material made of unidirectional fibers embedded in a matrix. Let axis $\overline{\imath}_1^*$ be oriented along the fiber direction, $\overline{\imath}_2^*$ in the transverse direction, and $\overline{\imath}_3^*$ is perpendicular to the plane of the thin sheet. Triad $\mathcal{I}^* = (\overline{\imath}_1^*, \overline{\imath}_2^*, \overline{\imath}_3^*)$ is called the fiber aligned triad and the superscript $(\cdot)^*$ will be used to indicate quantities measured in this triad.

If the diameter of the fiber is small compared to the thickness of the sheet, the material can be assumed to be a homogeneous, transversely isotropic material. The existence of individual fibers can be ignored: fibers and matrix materials are *smeared* into an equivalent, homogeneous, anisotropic material. For a linearly elastic, transversely isotropic material the constitutive laws reduce to eq. (2.70).

It will be assumed that the thin sheet of material is in a plane stress state, see section 1.3, *i.e.*, $\sigma_3^* \approx \tau_{13}^* \approx \tau_{23}^* \approx 0$. The constitutive laws expressed in compliance form are written in the following form

$$\begin{Bmatrix} \epsilon_1^* \\ \epsilon_2^* \\ \gamma_{12}^* \end{Bmatrix} = \begin{bmatrix} 1/E_1^* & -\nu_{21}^*/E_2^* & 0 \\ -\nu_{12}^*/E_1^* & 1/E_2^* & 0 \\ 0 & 0 & 1/G_{12}^* \end{bmatrix} \begin{Bmatrix} \sigma_1^* \\ \sigma_2^* \\ \tau_{12}^* \end{Bmatrix}. \tag{2.72}$$

The compliance matrix is expressed in terms of four constants, E_1^*, E_2^*, ν_{12}^*, and G_{12}^*, which are called the *engineering constants*. Note that the compliance matrix must be symmetric, thus $\nu_{12}^*/E_1^* = \nu_{21}^*/E_2^*$. This means that although five constants appear in the expression of the compliance matrix, one of, them say ν_{21}^*, can be computed from the other, and hence, is not an independent quantity.

The engineering constants can be readily measured experimentally. Consider a simple test where the composite is subjected to a known stress in the fiber direction only, σ_1^*, *i.e.*, $\sigma_2^* = \tau_{12}^* = 0$, as depicted in the left part of fig. 2.17. The first equation of (2.72) now reduces to $\epsilon_1^* = \sigma_1^*/E_1^*$. The strain in the fiber direction, ϵ_1^*, can be measured as a function of the applied stress, σ_1^*, by means of a strain gauge, and the modulus of elasticity is then computed as $E_1^* = \sigma_1^*/\epsilon_1^*$. Clearly, E_1^* is the modulus of elasticity of the material in the fiber direction.

The second equation of (2.72) becomes $\epsilon_2^* = -\nu_{12}\sigma_1^*/E_1^*$. The strain in the direction transverse to the fiber, ϵ_2^*, can also be measured by means of a strain gauge. Poisson's ratio now becomes $\nu_{12}^* = -E_1^*\epsilon_2^*/\sigma_1^*$.

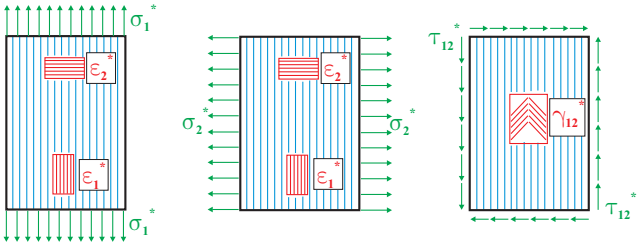

Fig. 2.17. Three simple tests for the determination of the engineering constants.

Consider next a second test where the composite material is subjected to a known stress in the direction transverse to the fiber, σ_2^*, *i.e.*, $\sigma_1^* = \tau_{12}^* = 0$, as depicted in the middle portion of fig. 2.17. Using the same approach as before, a measurement of the transverse strain, ϵ_2^*, as a function of the transverse stress, σ_2^*, will then yield E_2^*, the modulus of elasticity of the material in the direction transverse to the fiber. An additional measurement of the strain in the fiber direction, ϵ_1^*, will yield ν_{21}^*. The symmetry of the compliance matrix can be verified experimentally by checking that the various measured quantities satisfy the symmetry condition $\nu_{12}^*/E_1^* = \nu_{21}^*/E_2^*$, within the expected experimental errors.

Finally, in the last test, the composite material is subjected to a known shear stress, τ_{12}^*, only, *i.e.*, $\sigma_1^* = \sigma_2^* = 0$, as depicted in right portion of fig. 2.17. The last equation of (2.72) reduces to $\gamma_{12}^* = \tau_{12}^*/G_{12}^*$. A measurement of the shear strain, γ_{12}^*, then allows the evaluation of the shearing modulus, $G_{12}^* = \tau_{12}^*/\gamma_{12}^*$.

The stiffness matrix is obtained by inverting eq. (2.72) to find

$$\begin{Bmatrix} \sigma_1^* \\ \sigma_2^* \\ \tau_{12}^* \end{Bmatrix} = \begin{bmatrix} \dfrac{E_1^*}{1-\nu_{12}^{*2}E_2^*/E_1^*} & \dfrac{\nu_{12}^* E_2^*}{1-\nu_{12}^{*2}E_2^*/E_1^*} & 0 \\ \dfrac{\nu_{12}^* E_2^*}{1-\nu_{12}^{*2}E_2^*/E_1^*} & \dfrac{E_2^*}{1-\nu_{12}^{*2}E_2^*/E_1^*} & 0 \\ 0 & 0 & G_{12}^* \end{bmatrix} \begin{Bmatrix} \epsilon_1^* \\ \epsilon_2^* \\ \gamma_{12}^* \end{Bmatrix}. \tag{2.73}$$

To simplify the writing of the above relationships, the following stress and strain arrays are introduced

$$\underline{\sigma}^* = \left\{\sigma_1^*, \sigma_2^*, \tau_{12}^*\right\}^T, \quad \underline{\varepsilon}^* = \left\{\epsilon_1^*, \epsilon_2^*, \gamma_{12}^*\right\}^T. \tag{2.74}$$

The constitutive laws, eqs. (2.73) and (2.72), are written in compact form as

$$\underline{\sigma}^* = \underline{\underline{C}}^* \underline{\varepsilon}^*, \quad \text{and} \quad \underline{\varepsilon}^* = \underline{\underline{S}}^* \underline{\sigma}^*, \tag{2.75}$$

respectively. The stiffness and compliance matrices are then

$$\underline{\underline{C}}^* = \begin{bmatrix} \dfrac{E_1^*}{1-\nu_{12}^{*2}E_2^*/E_1^*} & \dfrac{\nu_{12}^* E_2^*}{1-\nu_{12}^{*2}E_2^*/E_1^*} & 0 \\ \dfrac{\nu_{12}^* E_2^*}{1-\nu_{12}^{*2}E_2^*/E_1^*} & \dfrac{E_2^*}{1-\nu_{12}^{*2}E_2^*/E_1^*} & 0 \\ 0 & 0 & G_{12}^* \end{bmatrix} = \begin{bmatrix} C_{11}^* & C_{12}^* & 0 \\ C_{12}^* & C_{22}^* & 0 \\ 0 & 0 & C_{66}^* \end{bmatrix}, \tag{2.76}$$

and

$$\underline{\underline{S}}^* = \begin{bmatrix} 1/E_1^* & -\nu_{21}^*/E_2^* & 0 \\ -\nu_{12}^*/E_1^* & 1/E_2^* & 0 \\ 0 & 0 & 1/G_{12}^* \end{bmatrix} = \begin{bmatrix} S_{11}^* & S_{12}^* & 0 \\ S_{12}^* & S_{22}^* & 0 \\ 0 & 0 & S_{66}^* \end{bmatrix}, \tag{2.77}$$

respectively.

The engineering constant for lamina made of a few different type of materials are listed in table 2.7. This table lists the volume fraction V_f, engineering constants E_1^*, E_2^*, ν_{12}^*, and G_{12}^*, as well as the density of the various lamina.

Table 2.7. Engineering constants for lamina made of different materials.

Material system	V_f	E_1^* [GPa]	E_2^* [GPa]	ν_{12}^*	G_{12}^* [GPa]	density [kg/m^3]
Graphite/Epoxy (T300/5208)	0.70	180.	10.	0.28	7.0	1600
Graphite/Epoxy (AS/3501)	0.66	138.	9.	0.30	7.0	1600
Boron/Epoxy (T300/5208)	0.50	204.	18.	0.23	5.6	2000
Scotchply (1002)	0.45	39.	8.	0.26	4.0	1800
Kevlar 49	0.60	76.	5.5	0.34	2.3	1460

2.6.2 Constitutive laws for a lamina in an arbitrary triad

In the previous section, the constitutive laws for a lamina made of a transversely isotropic material are discussed. The stresses and strains are measured in the fiber aligned triad, $\mathcal{I}^*$. In many cases, however, the constitutive laws for the lamina are required for a direction that might not coincide with that of the fibers. Figure 2.18 shows a transversely isotropic lamina with a reference triad, $\mathcal{I} = (\bar{\imath}_1, \bar{\imath}_2, \bar{\imath}_3)$ and the fiber aligned triad, $\mathcal{I}^*$. The fibers run at an angle θ with respect to a reference triad; angle θ is counted positive in the counterclockwise direction. Let $\underline{\sigma}$, and $\underline{\varepsilon}$ be the arrays of in-plane stresses and strains, respectively, measured in the reference triad $\mathcal{I}$. The lamina constitutive laws, measured in triad $\mathcal{I}$, now become

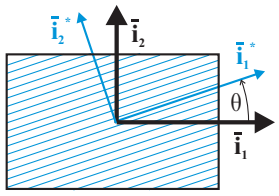

Fig. 2.18. Definition of two axis systems for a lamina.

$$\underline{\sigma} = \underline{\underline{C}}\,\underline{\varepsilon}. \tag{2.78}$$

Stiffness matrix $\underline{\underline{C}}$ could be obtained experimentally by performing a series a tests on the lamina, applying a stress along axis $\bar{\imath}_1$ first, then along axis $\bar{\imath}_2$, as

described in the previous section. Although conceptually feasible, this approach is not practical because a series of tests would have to be performed each time the constitutive laws are desired for a specific angle θ. A better approach would be to relate the stiffness properties at an angle θ to those measured in the fiber direction. This can be readily achieved with the help of the formulae for computing stresses and strains in a rotated axis system.

Rotation of the stiffness matrix

All the elements required to relate the constitutive laws in the two triads are now in place. The constitutive laws for a lamina expressed in the fiber aligned triad, $\underline{\sigma}^* = \underline{\underline{C}}^* \underline{\varepsilon}^*$, are the starting point of the development. Introducing the rotation formulae for stresses, eq. (1.47), and strain, eq. (1.91), yields

$$\begin{bmatrix} m^2 & n^2 & 2mn \\ n^2 & m^2 & -2mn \\ -mn & mn & m^2-n^2 \end{bmatrix} \begin{Bmatrix} \sigma_1 \\ \sigma_2 \\ \tau_{12} \end{Bmatrix} = \underline{\underline{C}}^* \begin{bmatrix} m^2 & n^2 & mn \\ n^2 & m^2 & -mn \\ -2mn & 2mn & m^2-n^2 \end{bmatrix} \begin{Bmatrix} \epsilon_1 \\ \epsilon_2 \\ \gamma_{12} \end{Bmatrix},$$

where $m = \cos\theta$ and $n = \sin\theta$. Multiplying from the left by the inverse of the rotation matrix for stresses results in

$$\begin{Bmatrix} \sigma_1 \\ \sigma_2 \\ \tau_{12} \end{Bmatrix} = \begin{bmatrix} m^2 & n^2 & -2mn \\ n^2 & m^2 & 2mn \\ mn & -mn & m^2-n^2 \end{bmatrix} \underline{\underline{C}}^* \begin{bmatrix} m^2 & n^2 & mn \\ n^2 & m^2 & -mn \\ -2mn & 2mn & m^2-n^2 \end{bmatrix} \begin{Bmatrix} \epsilon_1 \\ \epsilon_2 \\ \gamma_{12} \end{Bmatrix}.$$

Comparing this relationship to (2.78) then leads to

$$\underline{\underline{C}} = \begin{bmatrix} m^2 & n^2 & -2mn \\ n^2 & m^2 & 2mn \\ mn & -mn & m^2-n^2 \end{bmatrix} \underline{\underline{C}}^* \begin{bmatrix} m^2 & n^2 & 2mn \\ n^2 & m^2 & -2mn \\ -mn & mn & m^2-n^2 \end{bmatrix}. \tag{2.79}$$

Performing this triple matrix multiplication yields the various terms of the stiffness matrix

$$C = \begin{bmatrix} C_{11} & C_{12} & C_{16} \\ C_{12} & C_{22} & C_{26} \\ C_{16} & C_{26} & C_{66} \end{bmatrix}, \tag{2.80}$$

where $C_{11} = m^4 C_{11}^* + n^4 C_{22}^* + 2m^2 n^2 C_{12}^* + 4m^2 n^2 C_{66}^*$ and similar expressions hold for the other entries. In view of the complexity of this result that involves powers of trigonometric functions, an alternative expression can be derived based on well-known trigonometric identities to find

$$\begin{aligned} C_{11} &= \alpha_1 + \alpha_2 + \alpha_3 \cos 2\theta + \alpha_4 \cos 4\theta, \\ C_{22} &= \alpha_1 + \alpha_2 - \alpha_3 \cos 2\theta + \alpha_4 \cos 4\theta, \\ C_{12} &= \alpha_1 - \alpha_2 - \alpha_4 \cos 4\theta, \\ C_{66} &= \alpha_2 - \alpha_4 \cos 4\theta, \\ C_{16} &= (\alpha_3/2) \sin 2\theta + \alpha_4 \sin 4\theta, \\ C_{26} &= (\alpha_3/2) \sin 2\theta - \alpha_4 \sin 4\theta, \end{aligned} \tag{2.81}$$

where the four material invariants, α_1, α_2, α_3, and α_4, are defined as

$$\alpha_1 = \frac{E_1^* + E_2^* + 2\nu_{12}^* E_2^*}{4\alpha_0}, \quad \alpha_2 = \frac{E_1^* + E_2^* - 2\nu_{12}^* E_2^*}{8\alpha_0} + \frac{G_{12}^*}{2}, \tag{2.82a}$$

$$\alpha_3 = \frac{E_1^* - E_2^*}{2\alpha_0}, \quad \alpha_4 = \frac{E_1^* + E_2^* - 2\nu_{12}^* E_2^*}{8\alpha_0} - \frac{G_{12}^*}{2}, \tag{2.82b}$$

and where $\alpha_0 = 1 - \nu_{12}^{*2} E_2^* / E_1^*$.

This relationship is written in a more compact manner by defining the following matrix

$$\underline{\underline{\chi}}(\theta) = \begin{bmatrix} 1 & 1 & \cos 2\theta & \cos 4\theta \\ 1 & 1 & -\cos 2\theta & \cos 4\theta \\ 1 & -1 & 0 & -\cos 4\theta \\ 0 & 1 & 0 & -\cos 4\theta \\ 0 & 0 & \frac{1}{2}\sin 2\theta & \sin 4\theta \\ 0 & 0 & \frac{1}{2}\sin 2\theta & -\sin 4\theta \end{bmatrix}, \tag{2.83}$$

which is a function of the lamina orientation angle only. Next, the array of stiffness component is defined as

$$\underline{C} = \left\{ C_{11}, C_{22}, C_{12}, C_{66}, C_{16}, C_{26} \right\}^T, \tag{2.84}$$

and finally, the array of material invariants

$$\underline{\alpha} = \left\{ \alpha_1, \alpha_2, \alpha_3, \alpha_4 \right\}^T. \tag{2.85}$$

With these notations, the entries of the stiffness matrix for a lamina with a fiber orientation angle θ can be written as

$$\underline{C}(\theta) = \underline{\underline{\chi}}(\theta)\underline{\alpha}. \tag{2.86}$$

In summary, the stiffness matrix for a lamina can be obtained as follows.

1. Determine the engineering constants, E_1^*, E_2^*, ν_{12}^*, and G_{12}^* by performing a series of test on the lamina, as discussed in section 2.6.1.
2. Compute the stiffness matrix, $\underline{\underline{C}}^*$, in the fiber aligned triad, see eq. (2.76).
3. Compute the material invariants, α_1, α_2, α_3, and α_4, with the help of eqs.(2.82). Set up the array of material invariants defined by eq. (2.85).
4. Set up matrix $\underline{\underline{\chi}}(\theta)$ given by eq. (2.83) for the desired fiber orientation angle, θ, and evaluate the components of the stiffness matrix using eq. (2.86).

The material invariants for lamina made of a few different type of materials are listed in table 2.8. This table lists the material invariants computed from eqs. (2.82) based on the data of table 2.7.

Figure 2.19 shows the stiffness components, C_{11} and C_{22}, as a function of the lamina angle, θ, for the Graphite/Epoxy T300/5208 material system. Note the rapid decline of the stiffness coefficient, C_{11}, when the lamina angle moves away from 0 degrees. This sharp decline is due to the high directionality of the lamina stiffness

Table 2.8. Material invariants for lamina made of different materials.

Material system	α_1 [GPa]	α_2 [GPa]	α_3 [GPa]	α_4 [GPa]
Graphite/Epoxy (T300/5208)	49.11	26.65	85.37	19.65
Graphite/Epoxy (AS/3501)	38.32	21.30	64.88	14.30
Boron/Epoxy (T300/5208)	57.84	29.64	93.44	24.04
Scotchply (1002)	12.97	7.43	15.72	3.43
Kevlar 49	21.49	10.95	35.55	8.65

properties. The shearing stiffness component, C_{66}, shown in fig. 2.20, drastically increases when the lamina angle is 45 degrees. This can be explained as follows: a state of pure shear, see section 1.3.5, is equivalent to stresses in tension and compression acting at 45 and 135 degree angles, respectively. Theses stresses are now aligned with the fiber direction, which presents very high stiffness.

The coupling stiffness terms, C_{16} and C_{26}, do not vanish. These terms express a coupling between extension and shearing of the lamina. In contrast, the stiffness matrix, $\underline{\underline{C}}^*$, expressed in the fiber aligned triad, has vanishing terms in the corresponding entries. Indeed, when the loading is applied along the fiber direction, which is the intersection of two planes of symmetry, the response of the system must be symmetric, precluding extension-shear coupling. When the loading is no longer aligned with the intersection of the two planes of symmetry, a coupled response of the lamina is intuitively expected. Figure 2.21 shows the stiffness components, C_{16} and C_{26}, as a function of lamina angle θ.

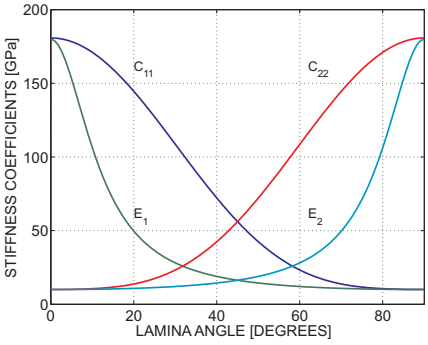

Fig. 2.19. Variation of the stiffness coefficients, C_{11} and C_{22}, and the engineering constants, E_1 and E_2, as a function of θ.

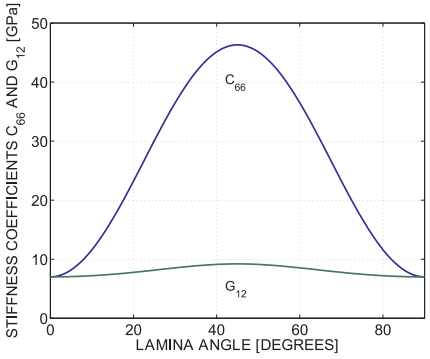

Fig. 2.20. Variation of the stiffness coefficient, C_{66}, and engineering constant, G_{12} as a function of θ.

Rotation of the compliance matrix

The lamina constitutive laws can be expressed in the stiffness form, eq. (2.78), or in the compliance form as

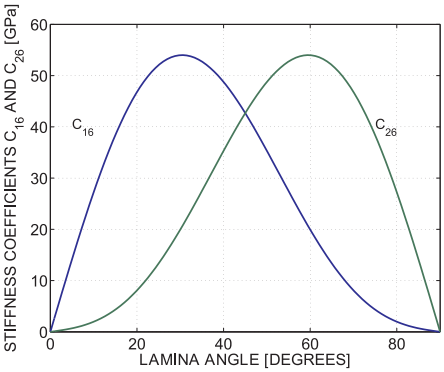

Fig. 2.21. Variation of the coupling stiffness coefficients, C_{16} and C_{26}, with the lamina angle θ.

$$\underline{\varepsilon} = \underline{\underline{S}}\,\underline{\sigma}, \tag{2.87}$$

where $\underline{\underline{S}} = \underline{\underline{C}}^{-1}$ is the compliance matrix measured in the arbitrary triad. Of course, the compliance matrix can be obtained by inverting the stiffness matrix, as indicated by eq. (2.65), but a direct determination is also possible. Introducing the stress rotation formula, eq. (1.47), and strain rotation formula, eq. (1.91), into the constitutive laws, eq. (2.75), and identifying the result with eq. (2.87) yields

$$\underline{\underline{S}} = \begin{bmatrix} m^2 & n^2 & -mn \\ n^2 & m^2 & mn \\ 2mn & -2mn & m^2-n^2 \end{bmatrix} \underline{\underline{S}}^* \begin{bmatrix} m^2 & n^2 & 2mn \\ n^2 & m^2 & -2mn \\ -mn & mn & m^2-n^2 \end{bmatrix}. \tag{2.88}$$

Performing this triple matrix multiplication yields the terms of the compliance matrix

$$\underline{\underline{S}} = \begin{bmatrix} S_{11} & S_{12} & S_{16} \\ S_{12} & S_{22} & S_{26} \\ S_{16} & S_{26} & S_{66} \end{bmatrix} = \begin{bmatrix} 1/E_1 & -\nu_{21}/E_2 & \nu_{61}/G_{12} \\ -\nu_{12}/E_1 & 1/E_2 & \nu_{62}/G_{12} \\ \nu_{16}/E_1 & \nu_{26}/E_2 & 1/G_{12} \end{bmatrix}, \tag{2.89}$$

where E_1, E_2, ν_{12}, G_{12}, ν_{16}, and ν_{26}, define the engineering constants in the arbitrary triad. Due to the symmetry of the compliance matrix, the following relationships hold $\nu_{12}/E_1 = \nu_{21}/E_2$, $\nu_{16}/E_1 = \nu_{61}/G_{12}$, and $\nu_{26}/E_2 = \nu_{62}/G_{12}$. The first entry of the compliance matrix is $S_{11} = m^4 S_{11}^* + n^4 S_{22}^* + 2m^2 n^2 S_{12}^* + m^2 n^2 S_{66}^*$, and similar expressions can be obtained for the other entries. In view of the complexity of this result that involves powers of trigonometric functions, an alternative expression is derived based on well-known trigonometric identities to find

$$\begin{aligned} S_{11} &= \beta_1 + \beta_2 + \beta_3 \cos 2\theta + \beta_4 \cos 4\theta, \\ S_{22} &= \beta_1 + \beta_2 - \beta_3 \cos 2\theta + \beta_4 \cos 4\theta, \\ S_{12} &= \beta_1 - \beta_2 - \beta_4 \cos 4\theta, \\ S_{66} &= 4\beta_2 - 4\beta_4 \cos 4\theta, \\ S_{16} &= \beta_3 \sin 2\theta + 2\beta_4 \sin 4\theta, \\ S_{26} &= \beta_3 \sin 2\theta - 2\beta_4 \sin 4\theta, \end{aligned} \tag{2.90}$$

where the material invariants, β_1, β_2, β_3, and β_4, are defined as

$$\beta_1 = \frac{1}{4}\left(\frac{1}{E_1^*} + \frac{1}{E_2^*} - \frac{2\nu_{12}^*}{E_1^*}\right), \quad \beta_2 = \frac{1}{8}\left(\frac{1}{E_1^*} + \frac{1}{E_2^*} + \frac{2\nu_{12}^*}{E_1^*}\right) + \frac{1}{8G_{12}^*}, \tag{2.91a}$$

$$\beta_3 = \frac{1}{2}\left(\frac{1}{E_1^*} - \frac{1}{E_2^*}\right), \qquad \beta_4 = \frac{1}{8}\left(\frac{1}{E_1^*} + \frac{1}{E_2^*} + \frac{2\nu_{12}^*}{E_1^*}\right) - \frac{1}{8G_{12}^*}. \tag{2.91b}$$

Explicit expression for the engineering constants can be obtained from eq. (2.89)

$$E_1 = 1/\left(\beta_1 + \beta_2 + \beta_3 \cos 2\theta + \beta_4 \cos 4\theta\right), \tag{2.92a}$$

$$E_2 = 1/\left(\beta_1 + \beta_2 - \beta_3 \cos 2\theta + \beta_4 \cos 4\theta\right), \tag{2.92b}$$

$$\nu_{12} = -\left(\beta_1 - \beta_2 - \beta_4 \cos 4\theta\right) / \left(\beta_1 + \beta_2 + \beta_3 \cos 2\theta + \beta_4 \cos 4\theta\right), \tag{2.92c}$$

$$G_{12} = 1/\left(4\beta_2 - 4\beta_4 \cos 4\theta\right), \tag{2.92d}$$

$$\nu_{16} = \left(\beta_3 \sin 2\theta + 2\beta_4 \sin 4\theta\right) / \left(\beta_1 + \beta_2 + \beta_3 \cos 2\theta + \beta_4 \cos 4\theta\right), \tag{2.92e}$$

$$\nu_{26} = \left(\beta_3 \sin 2\theta - 2\beta_4 \sin 4\theta\right) / \left(\beta_1 + \beta_2 + \beta_3 \cos 2\theta + \beta_4 \cos 4\theta\right). \tag{2.92f}$$

These engineering constants can also be measured experimentally by performing the various tests depicted in fig. 2.22. The tests are similar to those discussed in section 2.6.1, except for the fact that stresses are now applied at an angle θ with respect to the fibers.

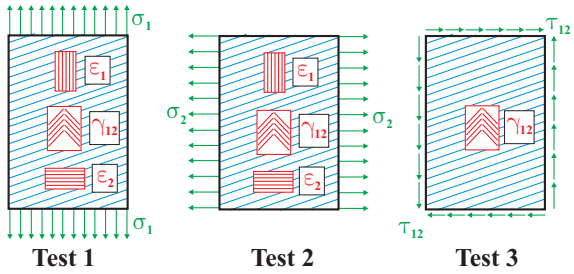

Fig. 2.22. Three simple tests for the determination of the engineering constants.

Figure 2.19 shows the variation of the modulus of elasticity, E_1, as a function of the lamina angle θ. Note the precipitous drop in the modulus of elasticity when the lamina angle moves away from 0 degrees. This drop is much more pronounced than that of the stiffness coefficient, C_{11}.

It is important to understand the difference between the stiffness coefficient, C_{11}, and the engineering constant, E_1. Mathematically, these two quantities clearly are different: $E_1 = 1/S_{11}$ but $1/S_{11} \neq C_{11}$ because the inverse of a matrix is not simply the inverse of its terms. This difference is easily understood in physical terms by looking at the tests that would allow the measurement of these quantities. Figure 2.22 shows the tests to be performed to measure the engineering constants, and fig. 2.23 shows the corresponding tests to be performed to measure the stiffness coefficients.

Focusing on the first test depicted in fig. 2.22, a single stress component, σ_1, is applied, *i.e.*, $\sigma_2 = \tau_{12} = 0$. A complex state of strain results that involves ϵ_1, ϵ_2, and γ_{12}. The measurement of the strain component, ϵ_1, yields E_1 from the first eq. (2.87), the measurement of ϵ_2 yields ν_{12} from the second eq. (2.87), and the measurement of γ_{12} yields ν_{16} from the last eq. (2.87).

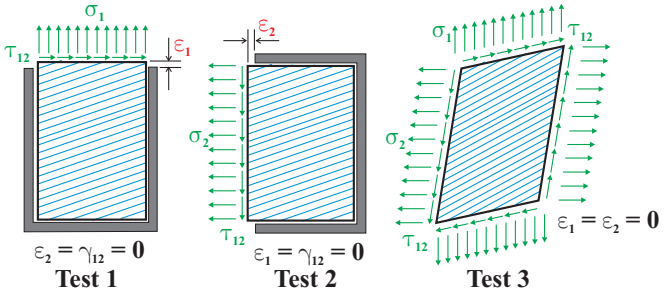

Fig. 2.23. Three simple tests for the determination of the stiffness coefficients.

In the first test depicted in fig. 2.23, a single strain component, ϵ_1, is applied, *i.e.*, $\epsilon_2 = \gamma_{12} = 0$. A complex state of stress results that involves stress components σ_1, σ_2, and τ_{12}. Measurements of these stresses would yield the stiffness coefficients, C_{11}, C_{12}, and C_{16}, from the first, second, and last equation of eqs. (2.78), respectively. Although conceptually simple, the tests depicted in fig. 2.23 are very difficult to perform in practice. For the first test, the test specimen would have to be constrained to prevent any deformations except for strain component ϵ_1, and the resulting stresses components would then need to be measured. Furthermore, friction between the sample and the side restraints should be completely eliminated. Clearly, such test is difficult to perform in practice.

Considering the first test in fig. 2.23 it is clear that the stiffness coefficient, C_{11}, reflects the stiffness of the material when it is constrained, *i.e.*, when $\epsilon_2 = \gamma_{12} = 0$. The effect of these constraints is to considerably stiffen the response of the material. At a 20 degree lamina angle, the stiffness coefficient C_{11} is about 130 GPa, see fig. 2.19, whereas the engineering constant E_1 is only about 50 GPa. The effect of constraining the material is clearly very important.

A similar effect is observed in fig. 2.19, which compares the stiffness coefficient, C_{66}, and the shearing modulus, G_{12}. The stiffness coefficient increases considerably, whereas the shearing modulus rises very modestly. Both quantities, however, reach their maximum values for a 45 degree lamina angle.

Figure 2.24 shows the Poisson's ratios, ν_{12}, and ν_{21}. Poisson's ratio ν_{12} has a value of 0.28 at a 0 degree lamina angle, but a value of about 0.02 only for a 90 degree lamina angle. For most metals, Poisson's ratio is about 0.3; with composite materials, a much wider range of value is observed. Finally, fig. 2.24 also shows the variation of the engineering constants ν_{16}, ν_{61}, ν_{26}, and ν_{62} as a function the lamina angle.

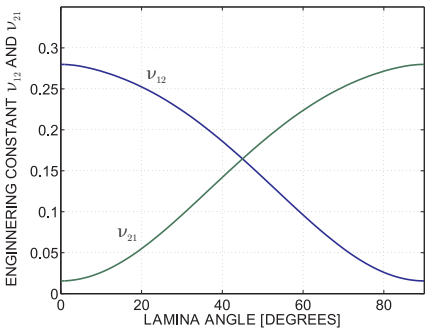

Fig. 2.24. Variation of engineering constants ν_{12} and ν_{21} with lamina angle θ.

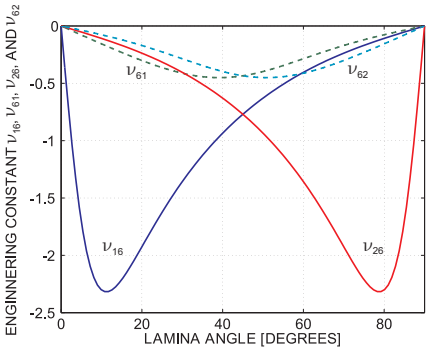

Fig. 2.25. Variation of engineering constants ν_{16}, ν_{61}, ν_{26}, and ν_{62} with lamina angle θ.

2.7 Strength of a transversely isotropic lamina

The constitutive laws for a linearly elastic, transversely isotropic material are investigated in section 2.6.2. The equations developed in that section express a linear relationship between stress and strain, but provide no information about the strength of the material.

2.7.1 Strength of a lamina under simple loading conditions

The strength of a lamina made of transversely isotropic material can be experimentally determined by performing a series of simple tests. In practical applications, this lamina will be under plane state of stress. Consider a first test where the lamina is subjected to a single tensile stress, σ_1^*, applied in the fiber direction, *i.e.*, $\sigma_2^* = \tau_{12}^* = 0$, as depicted in fig. 2.26. As the applied stress increases, a point is reached where the material fails. Let σ_{1t}^{*f} be the stress level at which failure occurs. The same test could be repeated for a compressive stress σ_1^*, and let σ_{1c}^{*f} be the absolute value of the compressive stress at failure. There is no reason to believe that σ_{1t}^{*f} and σ_{1c}^{*f} are, in general, equal. Therefore, the subscripts $(.)_t$ and $(.)_c$ will be used to distinguish the tensile and compressive failure stresses, respectively.

In a second test, depicted in fig. 2.26, the lamina is subjected to a single tensile stress, σ_2^*, applied in the direction transverse to the fiber, *i.e.*, $\sigma_1^* = \tau_{12}^* = 0$. The applied stress level that corresponds to failure of the lamina is denoted σ_{2t}^{*f}, and let σ_{2c}^{*f} be the absolute value of the compressive stress that corresponds to failure. Figure 2.26 also shows the third test to be performed in which the lamina is subjected to a shear stress, τ_{12}^*, whereas $\sigma_1^* = \sigma_2^* = 0$. Let τ_{12}^{*f} denote the level of applied shear stress that corresponds to failure. Clearly, the failure level in shear does not depend on the sign of the shear stress.

Although conceptually simple, the above tests can be very difficult to perform in practice. Care must be taken in the tensile tests to reinforce the ends of the test

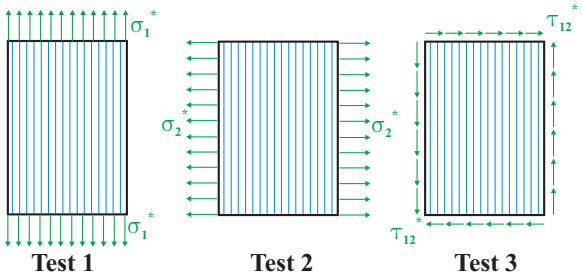

Fig. 2.26. Three tests for the determination of the strength of a lamina

specimens that fit into the grips of the testing machine to avoid premature failure near the grips. Furthermore, the specimen must be long enough to ensure that the test section is free of end effects. The test setup to measure compressive strength is far more complex because buckling of the specimen must be prevented. This can be achieved by providing lateral support of the test sample. Performing the shear test is also very complex. Subjecting a flat specimen to a state of pure shear is very difficult to achieve experimentally. Of course, a tubular specimen can be used, but at a far greater cost. Table 2.9 lists the typical failure stress levels for lamina made of different materials.

Table 2.9. Typical failure stresses for lamina made of different materials.

Material system	σ_{1t}^{*f} [MPa]	σ_{1c}^{*f} [MPa]	σ_{2t}^{*f} [MPa]	σ_{1c}^{*f} [MPa]	τ_{12}^{*f} [MPa]
Graphite/Epoxy (T300/5208)	1500	1500	40	240	68
Graphite/Epoxy (AS/3501)	1450	1450	52	205	93
Boron/Epoxy (T300/5208)	1260	2500	61	202	67
Scotchply (1002)	1060	610	31	118	72
Kevlar 49	1400	235	12	53	34

2.7.2 Strength of a lamina under combined loading conditions

In practical design situations, the lamina might be subjected to several stress components simultaneously. Consider, for instance, a lamina subjected to stresses along both the fiber direction and the transverse direction. Figure 2.27 shows the corresponding stress space and the failure stress levels σ_{1t}^{*f}, σ_{1c}^{*f}, σ_{2t}^{*f}, and σ_{2c}^{*f} which correspond to the various failure stress levels measured in the tests described previously. Assume that equal stresses are applied in both directions simultaneously, *i.e.*, $\sigma_1^* = \sigma_2^*$. These stress states form a 45 degree line in the stress space. As the applied stresses increase, failure will occur at a certain level. Of course, the applied stresses σ_1^* and σ_2^* could be applied in any proportion, corresponding to various ra-

dial lines emanating from the origin of the stress space. A different failure level will correspond to each radial line.

To cover all possible combinations, the failure envelope, depicted in fig. 2.27, should be known. All stress states within the failure envelope correspond to stress levels the material can sustain without failing, whereas the stress states outside the failure envelope result in failure.

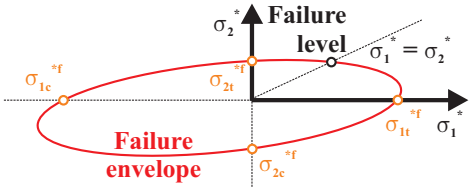

Fig. 2.27. Stress space for a lamina in biaxial stress state.

Clearly, the failure envelope could be obtained experimentally by performing a large number of tests with various combinations of applied stress components, σ_1^*, σ_2^*, and τ_{12}^*. This approach is not practical because it would require an overwhelming amount of testing to determine the failure envelope. A more desirable approach would be to determine the failure envelope based on the knowledge of a few failure stress levels such as σ_{1t}^{*f}, σ_{1c}^{*f}, σ_{2t}^{*f}, σ_{1c}^{*f}, and τ_{12}^{*f}. This can be achieved by means of a failure criterion that predicts failure under combined loads. Although many different failure criteria have been proposed, none is fully satisfactory, in the sense that their predictions are not always in very good agreement with the experimentally measured failure stresses. They are, however, widely used in preliminary design.

It is important to note that when designing with composite materials, the failure mode is often as important as the failure stress. Indeed, consider the case of a lamina subjected to a load transverse to the fibers: the lamina will fail at a very low stress level which is indicative of the low load carrying capability of the matrix material. On the other hand, if the same lamina is subjected to a stress aligned with the fibers, it will fail at a far higher stress level which reflects the high strength of the fiber. The failure modes in the two cases are quite different: matrix failure for the former, fiber failure for the latter. Failure of the matrix due to a transverse load does not substantially decrease the ability of the lamina to continue to carry high loads in the fiber direction, whereas with fiber failure, load carrying capability is completely lost. Clearly, a matrix failure is not always a catastrophic event in contrast to fiber failure, which completely eliminates any load carrying capability.

2.7.3 The Tsai-Wu failure criterion

A commonly used failure criterion is the Tsai-Wu failure criterion. This criterion states that the failure condition is reached when the combined applied stresses satisfy the following equality

$$F_{11}^{*}\sigma_{1}^{*2}+2F_{12}^{*}\sigma_{1}^{*}\sigma_{2}^{*}+F_{22}^{*}\sigma_{2}^{*2}+F_{66}^{*}\tau_{12}^{*2}+F_{1}^{*}\sigma_{1}^{*}+F_{2}^{*}\sigma_{2}^{*}=1, \tag{2.93}$$

where the coefficients F_{11}^{*}, F_{12}^{*}, F_{22}^{*}, F_{66}^{*}, F_{1}^{*}, and F_{2}^{*} must be determined experimentally. Note that the stress components appearing in the criterion are expressed in the fiber aligned triad. Consider first the test described earlier where a single stress component σ_{1}^{*} is applied. At failure in tension and in compression, the above equality must be satisfied, implying

$$F_{11}^{*}\sigma_{1t}^{*f2}+F_{1}^{*}\sigma_{1t}^{*f}=1, \quad F_{11}^{*}\sigma_{1c}^{*f2}-F_{1}^{*}\sigma_{1c}^{*f}=1.$$

The second test involves stress component σ_{2}^{*} only and yields

$$F_{22}^{*}\sigma_{2t}^{*f2}+F_{2}^{*}\sigma_{2t}^{*f}=1, \quad F_{22}^{*}\sigma_{2c}^{*f2}-F_{2}^{*}\sigma_{2c}^{*f}=1.$$

Finally, the last test involves τ_{12}^{*} only and implies $F_{66}^{*}\tau_{12}^{*f2}=1$. These five equations can be solved for five of the coefficients appearing in eq. (2.93) to find

$$F_{11}^{*}=\frac{1}{\sigma_{1t}^{*f}\sigma_{1c}^{*f}}, \quad F_{22}^{*}=\frac{1}{\sigma_{2t}^{*f}\sigma_{2c}^{*f}}, \quad F_{66}^{*}=\frac{1}{\tau_{12}^{*f2}};$$

$$F_{1}^{*}=\frac{\sigma_{1c}^{*f}-\sigma_{1t}^{*f}}{\sigma_{1t}^{*f}\sigma_{1c}^{*f}}, \quad F_{2}^{*}=\frac{\sigma_{2c}^{*f}-\sigma_{2t}^{*f}}{\sigma_{2t}^{*f}\sigma_{2c}^{*f}}.$$

These results are introduced in the initial statement of the failure criterion, eq. (2.93), to yield

$$\bar{\sigma}_{11}^{*2}+2\bar{F}_{12}^{*}\bar{\sigma}_{11}^{*}\bar{\sigma}_{22}^{*}+\bar{\sigma}_{22}^{*2}+\bar{\tau}_{12}^{*2}+\bar{F}_{1}^{*}\bar{\sigma}_{11}^{*}+\bar{F}_{2}^{*}\bar{\sigma}_{22}^{*}=1, \tag{2.94}$$

where the following non-dimensional stress components are defined,

$$\bar{\sigma}_{11}^{*}=\frac{\sigma_{1}^{*}}{\sqrt{\sigma_{1t}^{*f}\sigma_{1c}^{*f}}}; \quad \bar{\sigma}_{22}^{*}=\frac{\sigma_{2}^{*}}{\sqrt{\sigma_{2t}^{*f}\sigma_{2c}^{*f}}}; \quad \bar{\tau}_{12}^{*}=\frac{\tau_{12}^{*}}{\tau_{12}^{*f}}; \tag{2.95}$$

as well as the following non-dimensional coefficients:

$$\bar{F}_{1}^{*}=\frac{\sigma_{1c}^{*f}-\sigma_{1t}^{*f}}{\sqrt{\sigma_{1t}^{*f}\sigma_{1c}^{*f}}}; \quad \bar{F}_{2}^{*}=\frac{\sigma_{2c}^{*f}-\sigma_{2t}^{*f}}{\sqrt{\sigma_{2t}^{*f}\sigma_{2c}^{*f}}}. \tag{2.96}$$

Coefficient $\bar{F}_{12}^{*}$ is as yet undetermined. Clearly, an additional test involving a biaxial state of applied stress (*i.e.*, a test where both σ_{1}^{*} and σ_{2}^{*} are applied simultaneously) is required to determine this coefficient. Because such a biaxial test is very difficult to perform, coefficient $\bar{F}_{12}^{*}$ is often selected by fitting the prediction of the criterion to available experimental data. $\bar{F}_{12}^{*}=-1/2$ has been found to provide the best fit. The final statement of the Tsai-Wu criterion becomes

$$\bar{\sigma}_{11}^{*2}-\bar{\sigma}_{11}^{*}\bar{\sigma}_{22}^{*}+\bar{\sigma}_{22}^{*2}+\bar{\tau}_{12}^{*2}+\bar{F}_{1}^{*}\bar{\sigma}_{11}^{*}+\bar{F}_{2}^{*}\bar{\sigma}_{22}^{*}=1. \tag{2.97}$$

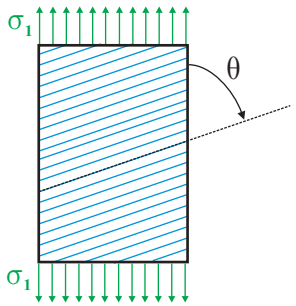

Fig. 2.28. Strength test for a lamina at an angle θ.

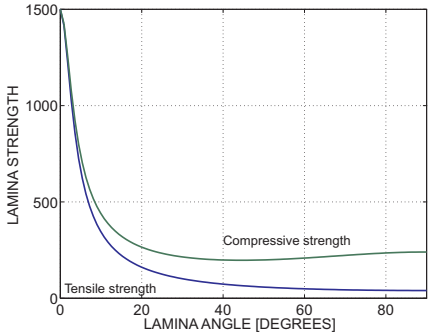

Fig. 2.29. Variation of the tensile and compressive failure loads with lamina angle θ.

Example 2.3. Tsai-Wu failure criterion for uniaxial stress

As an example of application of this criterion consider the simple test shown in fig. 2.28. A single stress component, σ_1, is applied to a lamina with fibers running at an angle θ. The stress rotation formula (1.47) yields the applied stresses in the fiber aligned triad as $\sigma_1^* = \sigma_1 \ \cos^2\theta$, $\sigma_2^* = \sigma_1 \ \sin^2\theta$, and $\tau_{12}^* = -\sigma_1 \ \cos\theta \sin\theta$.

The level of applied stress that corresponds to failure satisfies the failure criterion 2.97, *i.e.*,

$$\sigma_1^2 \left[\frac{\cos^4\theta}{\sigma_{1t}^{*f}\,\sigma_{1c}^{*f}} - \frac{\sin^2\theta\cos^2\theta}{\sqrt{\sigma_{1t}^{*f}\,\sigma_{1c}^{*f}\,\sigma_{2t}^{*f}\,\sigma_{2c}^{*f}}} + \frac{\sin^4\theta}{\sigma_{2t}^{*f}\,\sigma_{2c}^{*f}} + \frac{\sin^2\theta\cos^2\theta}{\tau_{12}^{*f2}} \right]$$
$$+ \sigma_1 \left[\frac{\bar{F}_1^*\cos^2\theta}{\sqrt{\sigma_{1t}^{*f}\,\sigma_{1c}^{*f}}} + \frac{\bar{F}_2^*\sin^2\theta}{\sqrt{\sigma_{2t}^{*f}\,\sigma_{2c}^{*f}}} \right] - 1 = 0.$$

This second order equation can be solved to find the failure load. The two solutions correspond to the failure loads in tension and compression. Figure 2.29 shows the absolute value of these failure loads as a function of the lamina angle θ for the Graphite/Epoxy materials (T300/5208) whose properties are given in table 2.9. Note the precipitous drop in strength as the lamina angle moves away from 0 degrees.

2.7.4 The reserve factor

The concept of reserve factor is often used in stress computations. The reserve factor, R, is defined as the factor by which the applied stress can be multiplied to reach failure, *i.e.*,

$$\sigma_{\text{fail}} = R\,\sigma_{\text{appl}}. \tag{2.98}$$

From this definition it follows that:

- $R = 1$ means that the applied stresses causes failure;

- $R > 1$ means that the applied stresses level is safe, *i.e.*, it is below the failure level. A reserve factor of two means that the applied stresses can be doubled before failure occurs;
- $R < 1$ means that the applied stresses is above the failure stress.

Let σ_1^*, σ_2^*, and τ_{12}^* be the stresses applied to a lamina. By definition of the reserve factor, it follows that $R\sigma_1^*$, $R\sigma_2^*$, $R\tau_{12}^*$ is the stress level that will cause failure. Assuming failure can be predicted by the Tsai-Wu failure criterion, eq. (2.97), the failure condition can be written as

$$\frac{(R\sigma_1^*)^2}{\sigma_{1t}^{*f}\sigma_{1c}^{*f}} - \frac{(R\sigma_1^*)(R\sigma_2^*)}{\sqrt{\sigma_{1t}^{*f}\sigma_{1c}^{*f}\sigma_{2t}^{*f}\sigma_{2c}^{*f}}} + \frac{(R\sigma_2^*)^2}{\sigma_{2t}^{*f}\sigma_{2c}^{*f}} + \frac{(R\tau_{12}^*)^2}{\tau_{12}^{*f2}} + \bar{F}_1^* \frac{R\sigma_1^*}{\sqrt{\sigma_{1t}^{*f}\sigma_{1c}^{*f}}} + \bar{F}_2^* \frac{R\sigma_2^*}{\sqrt{\sigma_{2t}^{*f}\sigma_{2c}^{*f}}} - 1 = 0.$$

Introducing the non-dimensional stresses, eq. (2.95), and regrouping the powers of R yields the following quadratic equation for the reserve factor

$$\left(\bar{\sigma}_{11}^{*2} - \bar{\sigma}_{11}^*\bar{\sigma}_{22}^* + \bar{\sigma}_{22}^{*2} + \bar{\tau}_{12}^{*2}\right) R^2 + \left(\bar{F}_1^*\bar{\sigma}_{11}^* + \bar{F}_2^*\bar{\sigma}_{22}^*\right) R - 1 = 0. \tag{2.99}$$

This quadratic equation has two roots, R_1 and R_2, which are positive and negative, respectively. The positive root gives the failure stress level, and the negative root gives the failure stress level when the sign of the applied stresses is reversed. In general, $|R_1| \neq |R_2|$ since the failure stress level in tension and compression are different.